Neurobiology of Disease

Intracellular Accumulation of α-Synuclein Aggregates Promotes S-Nitrosylation of MAP1A Leading to Decreased NMDAR-Evoked Calcium Influx and Loss of Mature Synaptic Spines

Ryan D. Hallam,[1*] Brodie Buchner-Duby,[1*] Morgan G. Stykel,[1] Carla L. Coackley,[1] and Scott D. Ryan[1,2]

[1]Department of Molecular and Cellular Biology, University of Guelph, Guelph, Ontario N1G 2W1, Canada, and [2]Neurodegenerative Disease Center, Scintillon Institute, San Diego, California 92121

Cortical synucleinopathies, including dementia with Lewy bodies and Parkinson's disease dementia, collectively known as Lewy body dementia, are characterized by the aberrant aggregation of misfolded α-synuclein (α-syn) protein into large inclusions in cortical tissue, leading to impairments in proteostasis and synaptic connectivity and eventually resulting in neurodegeneration. Here, we show that male and female rat cortical neurons exposed to exogenous α-syn preformed fibrils accumulate large, detergent-insoluble, PS129-labeled deposits at synaptic terminals. Live-cell imaging of calcium dynamics coupled with assessment of network activity reveals that aberrant intracellular accumulation of α-syn inhibits synaptic response to glutamate through NMDARs, although deficits manifest slowly over a 7 d period. Impairments in NMDAR activity temporally correlated with increased nitric oxide synthesis and S-nitrosylation of the dendritic scaffold protein, microtubule-associated protein 1A. Inhibition of nitric oxide synthesis via the nitric oxide synthase inhibitor L-NG-nitroarginine methyl ester blocked microtubule-associated protein 1A S-nitrosylation and normalized NMDAR-dependent inward calcium transients and overall network activity. Collectively, these data suggest that loss of synaptic function in Lewy body dementia may result from synucleinopathy-evoked nitrosative stress and subsequent NMDAR dysfunction.

Key words: **alpha-synuclein; MAP1A; NMDAR; Parkinson's disease; S-nitrosylation; synapse**

Significance Statement

This work shows the importance of the redox state of microtubule-associated protein 1A in the maintenance of synaptic function through regulation of NMDAR. We show that α-syn preformed fibrils promote nitric oxide synthesis, which triggers S-nitrosylation of microtubule-associated protein 1A, leading to impairment of NMDAR-dependent glutamate responses. This offers insight into the mechanism of synaptic dysfunction in Lewy body dementia.

Introduction

Intracellular accumulation of α-syn results in impaired proteostasis and perturbations in neuronal function, including synaptic and mitochondrial dysfunction (Wong and Krainc, 2017). Sequestration of α-syn into aggregates has been reported in multiple cellular compartments, including the presynaptic (Iwai et al., 1995; Withers et al., 1997; Kahle et al., 2000a, 2000b; Kramer and Schulz-Schaeffer, 2007; Zhang et al., 2008; Colom-Cadena et al., 2017) and postsynaptic terminals (Fortin et al., 2004; Emanuele et al., 2016; Colom-Cadena et al., 2017; Shrivastava et al., 2020). While the role of α-syn aggregation in presynaptic dysfunction and altered synaptic vesicle release has been extensively studied (for review, see Sulzer and Edwards, 2019), the role of α-syn aggregation in postsynaptic remains poorly understood. There is mounting evidence that aggregated α-syn perturbs postsynaptic ion channels, which may further exacerbate synaptic deficits. For instance, postsynaptic densities may be particularly sensitive to pathologic accumulation of α-syn as acute passive infusion of α-syn preformed fibrils (PFFs) into hippocampal neurons inhibits mEPSCs within minutes (Wu et al., 2019), suggesting that small amounts of oligomerized intracellular α-syn at the postsynaptic terminus are sufficient to

Received Jan. 11, 2022; revised Oct. 11, 2022; accepted Nov. 6, 2022.

Author contributions: R.D.H., B.B.-D., M.G.S., and C.L.C. performed research; R.D.H., B.B.-D., and S.D.R. analyzed data; B.B.-D. and S.D.R. edited the paper; S.D.R. designed research; S.D.R. wrote the paper.

This work was supported in part by Canadian Institutes of Health Research 2014-685 to S.D.R.; Natural Sciences and Engineering Research Council of Canada RGO60805 and CRDPJ 490841-15 to S.D.R., CGSM to R.D.H., and PSSO and OGS to B.B.-D.; and Vanier Program to M.G.S. We thank Tinya Wang for technical assistance with DAF-FM; and Stuart Lipton for critical editing of this manuscript.

*R.D.H. and B.B.-D. contributed equally to this work.

The authors declare no competing financial interests.

Correspondence should be addressed to Scott D. Ryan at sryan03@uoguelph.ca.

https://doi.org/10.1523/JNEUROSCI.0074-22.2022

interfere with synaptic function. Several studies have sought to determine the basis for pathologic α-syn-induced postsynaptic dysfunction, and evidence suggests that the defect may relate to NMDAR functionality (Chen et al., 2015; Yang et al., 2016; Durante et al., 2019).

In addition to the effect of α-syn aggregates on ionotropic glutamate receptors (iGluRs), we and others have shown that prolonged α-syn accumulation leads to a time-dependent increase in nitric oxide (NO) and other reactive nitrogen species (RNS) (Cooper et al., 2006; Ryan et al., 2013; Kam et al., 2018; Stykel et al., 2018). RNS has been widely implicated in the pathogenesis of many neurodegenerative diseases, including synucleinopathies (Hunot et al., 1996; Eve et al., 1998). NO can react with the reactive oxygen species superoxide anion to produce the highly toxic peroxynitrite, an RNS capable of damaging lipids through peroxidation and proteins through cysteine oxidation (known as S-nitrosylation) and tyrosine nitration (Lipton et al., 1993; Picon-Pages et al., 2019). Furthermore, NO-related species can aberrantly S-nitrosylate and impair function of many synaptic proteins (Nakamura et al., 2013). Endogenous NO is typically maintained at low levels; however, NMDAR-dependent increases in intracellular calcium can drive NO production through enhanced neuronal NO synthase (nNOS) activity (Garthwaite et al., 1988; Hardingham and Fox, 2006). NO-related species then act through a feedback mechanism to reduce NMDAR hyperactivation by directly modifying NMDAR activity through S-nitrosylation of cysteine thiol groups on synaptic proteins, resulting in decreased ion channel opening and spine retraction, thereby limiting further calcium flux (Choi and Lipton, 2000). Thus, it is conceivable that α-syn accumulation may result in an acute increase in NMDAR activity and increased NO levels, subsequently resulting in S-nitrosylation of synaptic proteins and a long-term decrease in postsynaptic activation, thereby providing a mechanism consistent with observations of both increased and decreased NMDAR function in response to accumulation of α-syn aggregates (Volpicelli-Daley et al., 2011; Durante et al., 2019).

To determine whether intracellular accumulation of α-syn aggregates promotes NO-mediated loss of NMDAR activation in cortical neurons, we used the PFF model of evoked synucleinopathy that models fibrillogenesis (Mahul-Mellier et al., 2020), contrasted against a monomer exposure paradigm where fibrillogenesis is limited (Kim et al., 2019). Following exposure of primary cortical neurons to α-syn-PFFs, we observed an increase in pathologic α-syn deposits at synaptic terminals coupled to decreased spontaneous network activity. Moreover, α-syn-PFFs inhibited synaptic response to glutamate through NMDARs while having no effect on AMPAR-mediated responses. The effect on NMDAR activity was time-dependent, requiring up to 6 d to manifest and coincided with a loss of mature dendritic spines. Impairment in NMDAR activity was preceded by increased NO synthesis and S-nitrosylation of the dendritic scaffold, microtubule-associated protein 1A (MAP1A), forming SNO-MAP1A. Inhibition of NO synthesis via the NOS inhibitor L-NG-nitroarginine methyl ester (L-NAME) blocked SNO-MAP1A formation, normalized NMDAR-dependent calcium transients and spontaneous network activity, and rescued mature spine number. Collectively, these data offer a mechanism of α-syn-mediated impairment of NMDAR function suggesting that exposure to α-syn-aggregates leads first to NO generation that subsequently results in decreased NMDAR-activity and loss of synaptic function.

Materials and Methods

Chemicals. Chemicals used in this study were sourced from MilliporeSigma unless otherwise specified below.

Cell isolation culture. Primary cortical neurons were harvested from both male and female E18 Sprague Dawley rat embryos (Charles River). Following dissection, pooled tissue was digested using filter-sterilized 17 U/mg Papain (Sigma, P4762) solution and subjected to mechanical dissociation. Cells were seeded onto plates coated the previous day (0.15 mg/ml poly-D-lysine hydrobromide [Sigma, P0899] in sterile tissue culture grade water at 37°C for 24 h) and incubated at 37°C, 7.5% CO_2 until time of analysis. Alternating every 4 and 3 d, a 50% media change was performed using fresh primary culture media [(2% B27 supplement (Invitrogen, 17504044), 1% antibiotic/antimycotic (Cytiva, SV30079.01), 0.7% BSA Fraction V (Invitrogen, 50-121-5315), 0.1% β-mercaptoethanol (Invitrogen, 21985-023) in DMEM/F12 (Sigma, D8437)]. If required, at day 7, *in vitro* cells were treated with 1 μg/ml human α-syn PFFs, 1 μg/ml monomeric α-syn, or vehicle control (PBS). For dendritic spine analysis, neurons were transduced with with pLenti-Lifeact(Actin)-tdTomato (Addgene, 64048) at the time of plating. SH-SY5Y cells (ATCC, CRL-2266) were maintained at a low passage number (< 15) and free of mycoplasma contamination. Cells were were maintained in growth media [DMEM/F12 (Sigma, D8437) with 1% nonessential amino acids (HyClone SH30238.01), 1% pen/strep (Invitrogen, 15140122), 1% sodium pyruvate (Invitrogen 11360-070) containing 5% FBS (Atlanta Biologicals, S12450)]. SH-SY5Y differentiation was induced by reducing FBS concentration to 1% and adding 10 μM all-*trans*-retinoic acid (Thermo Fisher Scientific, catalog #AC207341000) for 7 d.

Formation of human recombinant α-syn preformed fibrils. Human α-syn protein was isolated from BL21-CodonPlus (DE3)-RIPL competent cells (Agilent, 230280) transformed with pET21a-α-synuclein (Addgene, 51486) and purified by sequential ion exchange FPLC and reversed-phase HPLC. Human α-syn PFFs were then generated as previously described (Volpicelli-Daley et al., 2011). Purified α-syn (5 mg/ml in PBS) was incubated at 37°C with constant shaking for 7 d, then aliquoted and stored at −80°C. Before use, PFFs were thawed and diluted in PBS, then subjected to sonication (20% amplitude, 30 s; 1 s on, 1 s off) and added to neuronal media for exposure to neurons at a concentration of 1 μg/ml. Both fibrillar and monomeric α-syn were analyzed by sedimentation assay to confirm separation of monomers from fibrils before use.

Immunofluorescence. At time of fixation, cells were washed with PBS and fixed with 4% PFA (Electron Microscopy Systems) in PBS for 5 min. Following fixation, cells were washed 3 times and then blocked for 1 h at room temperature with PBS + 3% BSA. Cells were then incubated overnight with primary antibody in PBS + 3% BSA. Primary antibodies were as follows: [Anti-PSD95 mouse monoclonal (Synaptic Systems catalog #124011); Anti-Bassoon mouse monoclonal (Abcam catalog #ab82958), Anti-Phosphoserine-129 (81A) rabbit monoclonal [EP1536Y] (Abcam catalog #ab51253), Anti-Alpha-synuclein aggregate rabbit monoclonal [MJFR-14-6-4-2] (Abcam catalog #ab209538)]. Cells were then washed 3 times with PBS, blocked with PBS + 3% BSA for 1 h at room temperature, and then incubated with AlexaFluor-conjugated secondary antibodies for 1 h at room temperature at a dilution of 1:2000. Secondaries were as follows: [Donkey anti-Mouse IgG (H&L) AlexaFluor-488 conjugate (Invitrogen, catalog #A21202); Donkey anti-Rabbit IgG (H&L) AlexaFluor-555 conjugate (Invitrogen, catalog #A32794)]. Cells were counterstained with DAPI (1:1000) and fluorescence imaging was performed using an LSM880 Airyscan confocal microscope (Carl Zeiss). Resolution was set at 140 nm laterally and 400 nm axially. Image acquisition was performed using ZEN version 2.6 (Carl Zeiss). The Pearson coefficient of colocalization was calculated on super-resolution 2D confocal images sets using colocalization module of ZEN version 2.6 (Carl Zeiss).

Dendritic spine analysis. Analysis of spine morphology and density was performed on cortical neurons expressing Lifeact(Actin)-tdTomato to identify spines from single neurons. Tracing was performed in Neurolucida 360 (MBF Bioscience) in a semiautomated manner. Experimenter input was primarily to resolve neurite intersections

from two independent neurons that could not be distinguished in an automated fashion. Four or five single neurons per field of acquisition were chosen at random, 3 fields per coverslip, and 9 independent experiments were analyzed. Experimenters were blind to the treatment conditions. To be scored as a spine, the filipodia required a minimum length of 2.5 μm. The morphology of dendritic spines were then classified into four different types based on the following parameters (set in Neurolucida360, MBF Bioscience): thin (the length of the spine is greater than the head diameter by a ratio >2.5:1 and the diameters of the head relative to the neck does not exceed ratio of 1:1.1), mushroom (the diameter of the head is greater than the diameter of the neck by a ratio of at least 3:1), stubby (the diameter of the head is similar to the total length of the spine (ratio <2.5:1), and branched (spines with two heads), in keeping with previous dendritic spine analyses conducted in rats (Chicurel and Harris, 1992; Harris et al., 1992; Bello-Medina et al., 2016). Spines on neurites within 60 μm of the soma were binned as proximal spines, while spines >60 μm from the soma were binned as distal consistent with previous reports on the effects of PFFs on spine density and synaptic activity *in vitro* (Wu et al., 2019).

Western blot analysis. Unless otherwise stated, all samples were lysed in ice-cold RIPA buffer containing protease and phosphatase inhibitors (10 mM PMSF, 1 mM aprotinin, 1 mM sodium orthovanadate, and 1 mM sodium fluoride). Samples were homogenized with an 18G needle and briefly centrifuged at 12,000 × *g* to remove cellular debris. The concentrations of the resulting protein lysates were determined using the Bio-Rad DC Protein Assay Kit as per the manufacturer's protocol. Proteins were separated by SDS-PAGE and then transferred onto 0.2 μm nitrocellulose membranes at 32 V overnight at 4°C. Blocking of membranes was performed for 1 h in a blocking buffer (5% nonfat dry milk or 5% BSA in PBS) with constant agitation. Primary antibodies were administered in blocking buffer and incubated overnight at 4°C with constant agitation. Primary antibodies were [mouse anti-α-syn (BD catalog #610787); mouse anti human-α-syn clone 211 (Abcam catalog #ab80627); Anti-Phosphoserine-129 (81A) rabbit monoclonal [EP1536Y] (Abcam catalog #ab51253)]; rabbit anti-GAPDH (Santa Cruz Biotechnology catalog #sc-25778); mouse anti-LC3B (Biolegend catalog #848802); rabbit anti-MAP1A (Abcam catalog #AB184349); rabbit anti-GRIN1 (Abcam catalog #ab109182); mouse anti-GRIN2B (BD catalog #610416); Rabbit anti-DYNLL2 (Novus catalog #NBP1-54377)]. Membranes were washed with PBS + 0.1% Tween 20, then blocked again with blocking buffer and probed with secondary antibody (dilution of 1:5000) in blocking buffer + 0.1% Tween 20 for 1 h at room temperature. Secondary antibodies were as follows: [Goat anti-Mouse IgG (H + L) Secondary Antibody, HRP (Thermo Fisher Scientific, catalog #31430); Goat anti-Rabbit IgG (H + L) Secondary Antibody, HRP (Thermo Fisher Scientific); LI-COR infrared-conjugated secondary/IRDye 800CW Donkey anti-Mouse IgG antibody (LI-COR Biosciences, catalog #926-32212); LI-COR infrared-conjugated secondary/IRDye 680RD Donkey anti-Rabbit IgG antibody (LI-COR Biosciences catalog #926-68073)]. If HRP-conjugated secondary antibodies were used, membranes were probed for 5 min with Clarity Western enhanced chemiluminescence blotting substrate (Bio-Rad) and visualized with photosensitive film. For LI-COR secondary antibodies, membranes were visualized with a LI-COR Odyssey Fc.

Detection of NO-related species by DAF-FM. Cells were loaded with 2.5 μM DAF-FM (Thermo Fisher Scientific, catalog #D23844) in recording buffer (in mM) as follows: 5 D-glucose, 10 HEPES, 135 NaCl, and 5 KCl. Briefly, cells were loaded with dye for 15 min at room temperature to permit de-esterification, live cell analysis was performed to track kinetics of NO synthesis by fluorescence imaging using an Axio Observer Z1 (Carl Zeiss) widefield microscope. All images were recorded at 30 s intervals. ROIs were drawn on each individual cell, and analysis was performed using the MeanROI function (ZEN version 2.6; Carl Zeiss) to determine the change in fluorescence over time. All data were normalized using the following equation: ΔF/F0, where F0 = mean fluorescence intensity at baseline (Time 0), F1 = mean fluorescence intensity subsequent times of acquisition, and ΔF = change in fluorescence intensity. The ΔF/F0 values from each ROI were used to calculate a mean ΔF/F0 for each independent experiment.

Bioinformatic analysis of NMDAR interactome. To identify known binding partners of the NMDAR complex, a protein interaction network analysis was performed using GeneMania 3.6.0 (accessed on June 29, 2021) (Warde-Farley et al., 2010), which contrasts targets against databases of known pathways in BioGRID, Reactome, and BioCyc, via PathwayCommons, and the resulting Homo sapiens "Physical Interaction" network was weighted based on biological process. Bait inputted was as follows: GRIN1, GRIN2A, GRIN2B, GRIN2C, GRIN3A, and GRIN3B. The resulting network map was generated by GeneMania 3.6.0.

Biotin switch assay. The biotin-switch assay is a modified immunoblot analysis used to detect the levels of S-nitrosylated proteins and has been described previously (Ryan et al., 2013). Briefly, SH-SY5Y cell lysates (500 μg to 1 mg) prepared in HENTS buffer (100 mM HEPES, pH 7.4, 1 mM EDTA, 0.1 mM Neocuproine, 1% Triton X-100, 0.1% SDS) or HENC buffer (250 mM HEPES, pH 7.4, 1 mM EDTA, 0.1 mM Neocuproine, 1% Triton X-100, 0.1% SDS, or 0.4% CHAPS) were mixed with blocking buffer (2.5% SDS, 10 mM methyl methane thiosulfonate [MMTS] in HEN buffer [250 mM HEPES, pH 7.4, 1 mM EDTA, and 0.1 mM Neocuproine]) and incubated for 30 min at 50°C with frequent vortexing to block free thiol groups. After removing excess MMTS by acetone precipitation, S-nitrosothiols were reduced to thiol with 20 mM ascorbate. Newly formed thiols were linked with the sulfhydryl-specific biotinylating reagent *N*-[6-(biotinamido)hexyl]-3′-(2′-pyridyldithio) propionamide (biotin-HPDP). Unreacted biotin-HPDP was removed and the pellet resuspended, neutralized, and centrifuged to clear undissolved debris. Five to ten percent of the supernatant was used as the input for the control blot, and biotinylated proteins pulled down with Neutravidin-agarose beads (Pierce) from the remaining supernatant. Beads were washed 5 times, eluted with glycine and resuspended in NuPAGE LDS sample buffer (Invitrogen), boiled at 95°C for 5 min, and analyzed by immunoblotting.

Soluble/insoluble α-syn fractionation. Primary cortical rat neurons treated for 7 DIV with monomeric α-syn or α-syn PFFs were collected in PBS and pelleted at 300 × *g* for 5 min. The pellets were resuspended in 1 ml of fractionation buffer (50 mM Tris-HCl, 750 mM NaCl, 10 mM NaF, 5 mM EDTA, 30% sucrose (w/v), 1% Triton X-100, pH 7.4) and homogenized with an 18G needle. Samples were then placed on sample rotator overnight at 4°C. The following day, samples were centrifuged at 100,000 × *g* for 30 min at 4°C to separate the soluble (supernatant) and insoluble (pellet) fractions. After removing the soluble fraction, the insoluble fraction was resuspended in 1:1 (v:v) fractionation buffer containing 8 M urea with 8% SDS (w/v) and analyzed by western blot.

Live-cell calcium imaging. To assess changes in calcium flux within neurons, Fluo-4 AM (Thermo Fisher Scientific, catalog #F14201) was used to visualize and quantify intracellular calcium concentrations. Before imaging, 14 DIV (7 d post-treatment) neurons on coverslips were washed with calcium buffer (HBSS, 2 mM calcium chloride, 2 mM glucose), loaded with 2.5 μM Fluo-4 AM (dissolved in DMSO) in calcium buffer, and incubated at room temperature in the dark for 30 min. Following dye loading, cells were washed twice with calcium buffer and incubated in calcium buffer for another 30 min to allow for de-esterification. Coverslips were then loaded into an imaging chamber and live-imaged using an Axio Observer Z1 (Carl Zeiss) widefield microscope at 37°C. Cells were allowed to stabilize for ~5 min and were then imaged for 2 min while in calcium buffer. All images were recorded at 250 ms intervals (four images/s). After 2 min, cells were then titrated with 10 ml of the various stimulants (20 μM glutamate, 100 μM NMDA, or 10 μM AMPA) dissolved in calcium buffer at a flow rate of ~0.5 ml/s with constant aspiration, and imaged for 1 min. ROIs were drawn on each individual cell body, and analysis was performed using the MeanROI function (ZEN version 2.6; Carl Zeiss) to determine the change in fluorescence over time. All data were normalized using the following equation: ΔF/F0, where F0 = mean fluorescence intensity at baseline, F1 = maximum fluorescence intensity following stimulation, and ΔF = change in fluorescence intensity. The ΔF/F0 values from each ROI were used to calculate a mean ΔF/F0 for each coverslip analyzed. Where indicated, pharmacological blockers were used to assess the relative contribution(s) of different receptor types. At the de-

esterification step, receptor blockers (1 mM $MgCl_2$, 10 μM MK-801, or 10 μM NBQX) were added to the calcium buffer and incubated with the cells for 30 min before analysis.

Multielectrode array recordings. Primary cortical neurons from E18 rat embryos were isolated as described above and seeded onto CytoView MEA 24-well plates (Axion Biosystems). Initial analysis was performed at 7 d after treatment with either α-syn monomers or PFFs using the Maestro Edge (Axion Biosystems). Plates were loaded and equilibrated for 5 min at 37°C, and electrical activity was recorded for 10 min. Following the first round of data acquisition, cells were treated with 1 mM L-NAME or vehicle and incubated for 24 h at 37°C and 7.5% CO_2. After the 24 h of incubation, cells were recorded again, and neural activity data were processed and exported for analysis (AxIS software, Axion Biosystems). Data from wells above the minimum threshold for activity, defined as having 5 or more spikes per minute on any electrode, were averaged; and the mean of all wells for each independent experiment was used to calculate a final average and SEM for each metric analyzed. Individual spikes, defined as an electrical signal exceeding the noise threshold set for each electrode (6× SD), were recorded and plotted as average weighted mean firing rate. Bursting was defined as a minimum of 5 spikes occurring in rapid succession with an interspike interval of <100 ms. As a measure for total synaptic connectivity, a mean synchrony index was calculated for each well, averaged between replicates, and then averaged for independent experiments (AxIS software, Axion Biosystems).

Experimental design and statistical analyses. All data are displayed as mean + SEM of independent experiments, except in the case of DAF-FM where data are expressed as mean ± SEM. For experiments wherein measurements were made on individual neurons (i.e., calcium imaging, DAF-FM, electrophysiological experiments, and spine counts), data were analyzed using a nested design whereby individual neurons were nested within replicates, nested within independent experiments. Data were analyzed using a two-way Student's *t* test when two groups were compared, a one-way ANOVA when three groups (or treatments) were compared, or a two-way ANOVA when groups (or treatments) were multifactorial. Statistical testing was performed using GraphPad Prism 9 (GraphPad Software). When a statistically significant difference was identified by ANOVA, *post hoc* Tukey's or Sidak's tests were performed where indicated. Tukey's test was used when differences between means of all groups were of interest, whereas Sidak's test was used when differences within groups from a larger dataset were of interest, such as examining the effect of treatment on spine number within each subclassification of spine. Degrees of statistical significance used are as follows: $^{*}p < 0.05$, $^{**}p < 0.01$.

Results

PFFs promote accumulation of α-syn aggregates in presynaptic and postsynaptic terminals

To evaluate the link between intracellular accumulation of α-syn aggregates and aberrant NMDAR activation, we used the PFF model of evoked synucleinopathy. The in-cell fibrilization of endogenous α-syn has been previously demonstrated to occur on exogenous addition of α-syn-PFFs to both primary neurons in culture (Luk et al., 2009; Volpicelli-Daley et al., 2014) and *in vivo* inoculation of the rodent striatum (Luk et al., 2012). Moreover, PFF evoked α-syn aggregation is dependent on endogenous α-syn expression as SNCA-KO animals show no response to PFF exposure (Luk et al., 2012). Neurons derived from E18 rat cortex were cultured for up to 14 DIV before being exposed to α-syn-PFFs, or either monomeric α-syn or PBS vehicle control. Neurons were tracked after PFF administration over a 15 d period. We found that PFF exposure resulted in recruitment of endogenous rat α-syn into multimeric aggregates at a rate significantly higher than that of monomeric α-syn (Fig. 1*A*,*B*). While multimeric α-syn levels peaked by 7 d after treatment and decreased thereafter, levels of α-syn phosphorylation at serine 129 (PS129) continued to rise, suggesting that acute PFF exposure has long-lasting effects on indices of α-syn pathology (Fig. 1*A*,*C*). Interestingly, monomeric exposure also impacted on the ratio of PS129 to total α-syn, although the kinetics of this effect were significantly reduced relative to PFF-exposed neurons (Fig. 1*A*,*C*). These effects are not likely to be the result of the persistent presence of human α-syn from exogenous exposure as the human α-syn added to cultures was largely cleared by 5 d after treatment in the case of monomeric α-syn and 7 d after treatment for α-syn-PFFs (Fig. 1*A*,*D*). To confirm that human α-syn was being degraded rapidly after exposure, neurons were treated with either MG132 to inhibit proteasomal clearance, choloroquine to inhibit lysosomal clearance, or a combination of the two (Fig. 1*E*,*F*). Clearance of monomeric α-syn was inhibited by both proteasomal and lysosomal inhibition, while PFF clearance was inhibited by lysosomal inhibition alone, consistent with reports that lysosomal degradation is the primary system involved in clearance of aggregated proteins (Dikic, 2017).

Defining characteristics of pathologic α-syn include both detergent insolubility and hyperphosphorylation (Volpicelli-Daley et al., 2011). To determine the biochemical characteristics of the α-syn aggregates present in cortical neurons, we performed a detergent-soluble (Triton X-100) versus detergent-insoluble (urea) protein fractionation on neurons 7 d after exposure to either PFFs or monomeric α-syn as this time point reflected minimal residual human α-syn and maximal endogenous multimeric α-syn. Using high-speed ultracentrifugation, the soluble and insoluble protein fractions were separated and solubilized. The monomeric form of α-syn was detected in both detergent-soluble and -insoluble fractions; whereas in PFF-exposed neurons, a large amount of mutimeric α-syn was detected in the detergent-insoluble fraction only (Fig. 1*G*,*H*). A modest increase in PS129-labeled insoluble protein was also observed (Fig. 1*G*,*I*). This demonstrates that PFF exposure results in a major shift in α-syn solubility that is commonly associated with a shift from soluble random coil or helical structures to aggregated β sheet. Despite the observed increase in total and PS129-labeled α-syn levels, no detectable aggregates were formed when nonfibrillized monomeric α-syn is added to neurons in culture.

Glutamate-evoked calcium influx is inhibited after PFF exposure

We next sought to determine the subcellular localization of these deposits and whether they are present at the synapse. Cortical neurons were transformed with LifeAct(Actin)-RFP, which permits visualization of dendritic spines, and exposed to α-syn-PFFs, or either monomeric α-syn or PBS vehicle controls. Seven day post exposure cells were fixed and immunolabeled for aggregated α-syn (Fig. 2*A*). We found that aggregated α-syn accumulated exclusively in neurons exposed to PFFs (Fig. 2*A*,*B*) and could be seen on dendritic spines. To confirm the synaptic localization of α-syn pathology, we labeled neurons with (PSD95) as a marker of the postsynaptic terminus or Bassoon as a marker of the presynaptic membrane, as well as hyperphosphorylated α-syn (PS129) as a marker of α-syn pathology a (PSD95) (Extended Data Fig. 2-1). We found that PFF-exposed neurons showed a dramatic increase in PS129 reactivity relative to monomeric α-syn-exposed neurons or PBS controls. Colocalization analysis indicated that PS129 deposition was consistent with both a presynaptic and postsynaptic localization (Extended Data Fig. 2-1*A*-*C*) 7 d after exposure to α-syn-PFFs.

Conflicting reports on whether α-syn inclusions increase or decrease NMDAR functionality led us to characterize the time-dependent effect of accumulating α-syn aggregates on synaptic function in glutamate responsive cortical neurons. Using Fluo-4 AM-based calcium imaging, we assessed spontaneous calcium transients and synaptic responses to glutamate in neurons 7 d

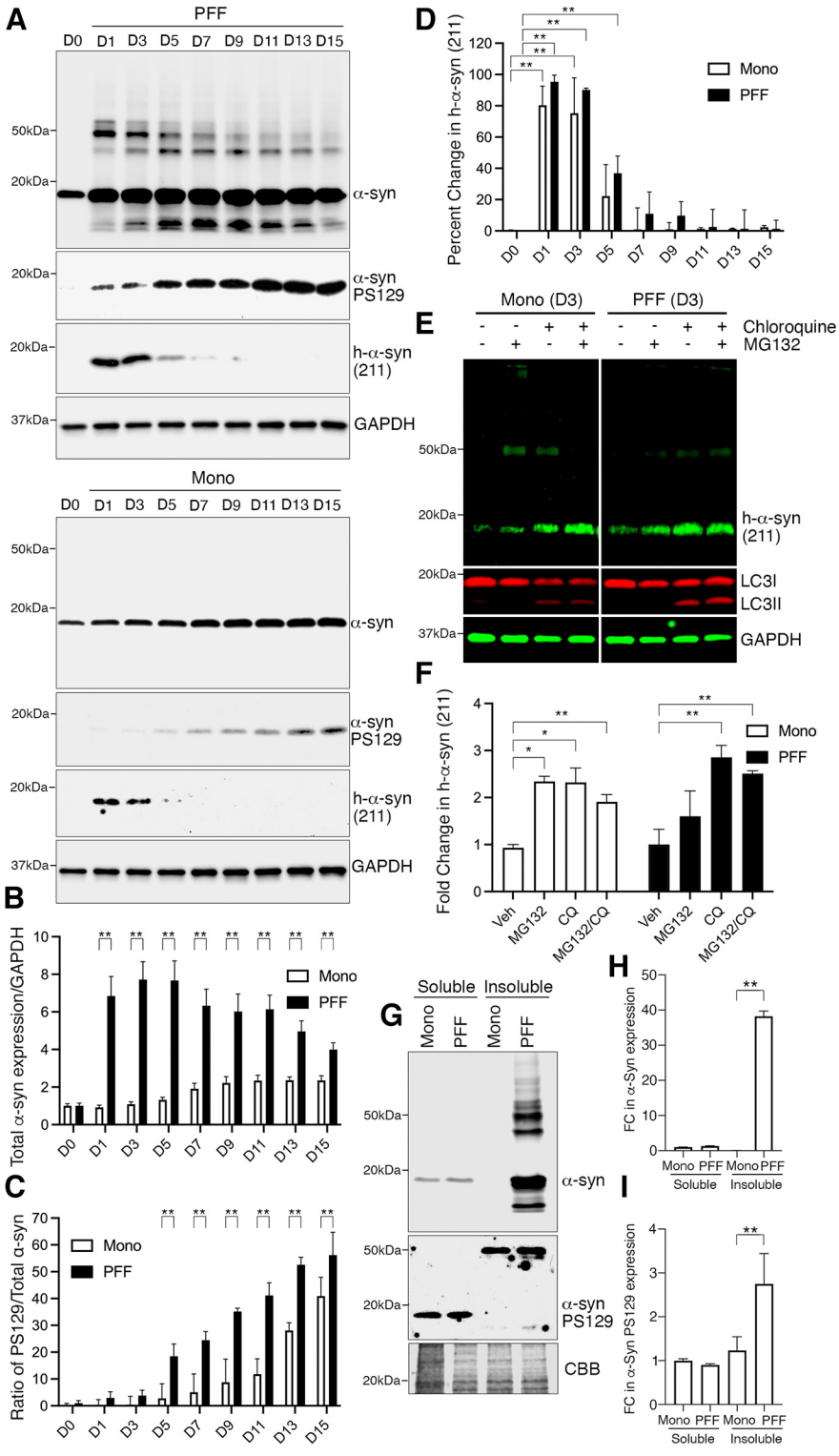

Figure 1. PFF exposure promotes accumulation of intracellular α-syn aggregates. ***A–D***, Rat cortical neurons exposed to α-syn-PFFs or α-syn monomers (***A***) showed increased accumulation of multimeric α-syn (***B***) and PS129 (***C***) relative to monomer-exposed neurons. Data are mean + SEM. $^{**}p < 0.01$ (two-way ANOVA with *post hoc* Sidak's test); $n = 9$. ***D***, Ectopic human α-syn monomers and PFFs are cleared from neurons within 5 and 7 d after administration, respectively. Data are mean + SEM. $^{**}p < 0.01$ (two-way ANOVA with *post hoc* Dunnett's test); $n = 6$. ***E***, ***F***, Ectopic human α-syn monomers accumulate following MG132 (5 μM) and/or chloroquine (20 μM) exposure, whereas PFFs accumulated following chloroquine exposure. Data are mean + SEM. $^{*}p < 0.05$; $^{**}p < 0.01$; two-way ANOVA with *post hoc* Tukey's test; $n = 6$. ***G–I***, Fractionation of proteins based on Triton X-100 (soluble) versus urea (insoluble) solubility (***G***) showed increased insoluble α-syn (***H***) and modestly increased insoluble PS129 α-syn (***I***) in PFFs exposed neurons relative to monomer (M) exposed. Data are mean + SEM. $^{**}p < 0.01$ (two-way ANOVA with *post hoc* Tukey's test); $n = 4$.

after PFF exposure by quantifying increases in intracellular calcium concentration following glutamate stimulation. We observed a significant decrease in spontaneous calcium bursts as a function of time in cortical neurons 7 d after PFF exposure relative to monomer- or PBS-exposed cells (Fig. 2*C*,*D*), indicative of impairments in network activity. Furthermore, a dramatic decrease in intracellular calcium flux was observed following glutamate stimulation in PFF-exposed neurons relative to monomeric α-syn control neurons (Fig. 2*E–G*). Representative traces of calcium influx in monomer-exposed neurons show strong glutamate responsiveness compared with baseline fluorescence, whereas PFF-treated neurons show a modest change in intracellular calcium fluorescence in response to glutamate (Fig. 2*F*). Quantification of the average fold change in calcium fluorescence over baseline and across multiple replicate cultures shows that there is a consistent and significant reduction in the response elicited by 20 μM glutamate 7 d after exposure to PFFs relative to PBS and monomer-exposed neurons (Fig. 2*G*).

We next sought to determine when inhibition of calcium influx was first detectable. We exposed neurons to PFFs and imaged immediately or at 24 h intervals after exposure. Immediately following PFF exposure, the baseline and post stimulation response to 20 μM glutamate were similar to those observed in monomer-exposed or PBS control neurons (Fig. 3*A–C*). This suggests that, under the conditions of this experiment, exogenous PFFs do not impede iGluR-mediated calcium influx following glutamate stimulation in cortical neurons. Tracking the response of these neurons to glutamate exposure at 24 h intervals after PFF exposure, we determined that PFF-evoked impairment in glutamate response was not evident until 6 d after exposure. This was consistent with the time needed for the levels of intracellular α-syn aggregates to plateau and for significant levels of PS129-labeled α-syn to accumulate (Fig. 1*A–C*). Collectively, these data argue that impaired glutamate-evoked calcium responses result from accumulation of intracellular PS129-labeled α-syn aggregates.

PFF exposure impairs calcium influx via NMDARs coincident with loss of mature dendritic spines

To characterize the observed deficit in glutamate-evoked synaptic responses, we focused on NMDAR and AMPAR, given the potential pleiotropic effects of α-syn inclusions with respect to activation of these receptors. We assessed specific iGluR-dependent

calcium influx, first through stimulation with either NMDA or AMPA 7 d after PFF exposure (Fig. 4*A*,*E*). Similar to the response observed following glutamate application, selective receptor stimulation with NMDA in the absence of Mg^{2+} showed reduced intracellular calcium concentrations in neurons after PFF exposure, relative to monomeric or PBS vehicle controls (Fig. 4*A*–*C*). Following selective AMPA stimulation, no significant difference in intracellular calcium flux was observed in any exposure paradigm (Fig. 4*E*–*G*), suggesting that the deficit was restricted to NMDAR-dependent signaling. To confirm this observation, neurons were stimulated with glutamate following selective NMDAR or AMPAR inhibition, to elicit calcium flux in the absence of target receptor activity. PFF-exposed neurons were stimulated with glutamate following a 30 min incubation with either an NMDAR-specific antagonist (MK-801), or an AMPAR-specific antagonist (NBQX), and subsequent calcium influx was monitored. Glutamate stimulation in the presence of MK-801 yielded a similar level of inhibition across all exposure paradigms (Fig. 4*D*), again suggesting these deficits are related to NMDAR activation. By contrast, NBQX inhibition of AMPARs did not alter responses under any exposure relative to glutamate alone (Fig. 4*H*), suggesting that AMPAR-mediated calcium influx is not altered by PFF exposure under these experimental conditions. Together, these results demonstrate that the perturbation of glutamate-evoked calcium flux is dependent on the inhibition of NMDAR function, while AMPAR function appears relatively unchanged. To assess whether synaptic dysfunction was related to anatomic changes in neuronal architecture, we next assessed the density of dendritic spines based on their morphologic classification over 7 d of exposure to either monomeric α-syn or PFFs. Primary cortical neurons were exposed to PFFs for up to 7 d, and the density of multiple morphologic classifications of dendritic spines was quantified at 24 h intervals. We observed a loss of mushroom-shaped dendritic spines following PFF exposure in both proximal and distal regions of the dendrite at 7 d after PFF exposure (Fig. 5*A*,*B*). Mushroom spines are generally thought to represent stable, mature synaptic connections, and are therefore critical to cognitive function

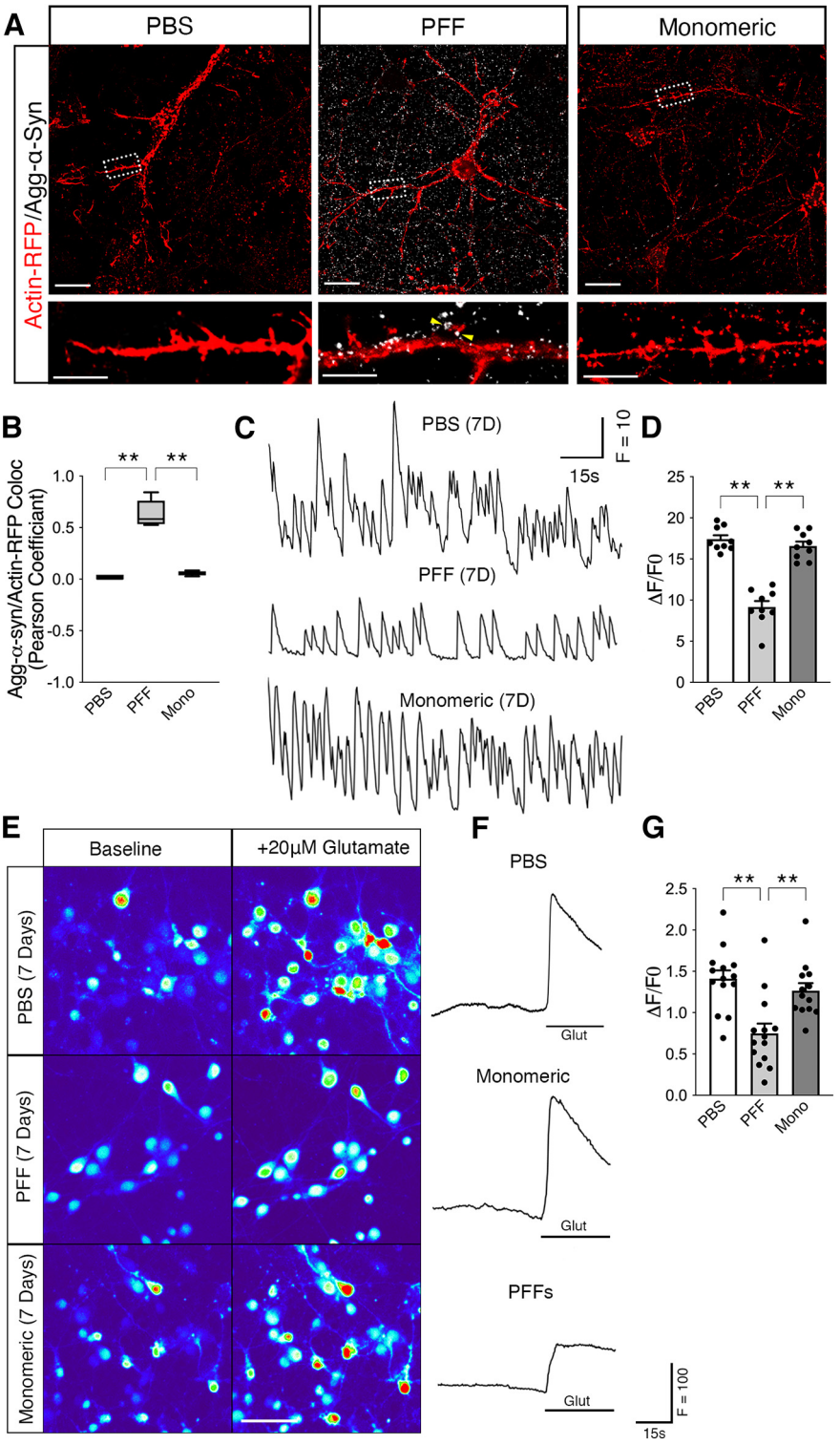

Figure 2. Glutamate-evoked calcium influx is inhibited after PFF exposure. ***A***, ***B***, LifeAct(Actin)-RFP expressing neurons were immunolabeled aggregated α-syn (agg-α-syn) following PBS, α-syn monomer, or PFF exposure. Data show a postsynaptic localization of α-syn pathology (see also Extended Data Fig. 2-1). Scale bar, 5 μm. Arrows point to agg-α-syn on dendritic spines. ***B***, Quantification of colocalization in ***A***. Data represent box-and-whisker plots of mean ± minimum and mean. $^{**}p < 0.01$ (ANOVA with *post hoc* Tukey); $n = 6$ independent experiments. ***C***, ***D***, Representative traces of spontaneous calcium transients in cortical neurons 7 d after PBS, PFF, or monomeric α-syn exposure (***C***). A significant reduction in the average number of intracellular calcium spikes per minute is observed after PFF exposure relative to control groups (***D***). Data are mean + SEM. $^{**}p < 0.01$ (two-way ANOVA with *post hoc* Tukey); $n = 9$ independent experiments. ***D–F***, Heatmap of representative micrographs depicts Fluo-4 AM fluorescence intensity in cortical neurons 7 d after PBS, PFF, or monomeric α-syn exposure, before and after stimulation with 20 μM glutamate (***E***). Representative traces of calcium transients show reduced calcium influx in response to 20 μM glutamate in neurons 7 d after PFF exposure (***F***). Quantification of average intracellular glutamate-evoked calcium flux shows a significant decrease in PFF-exposed neurons relative to PBS and monomeric α-syn controls (***G***). Data are mean + SEM. $^{**}p < 0.01$ (ANOVA with *post hoc* Tukey); $n = 14$ independent experiments.

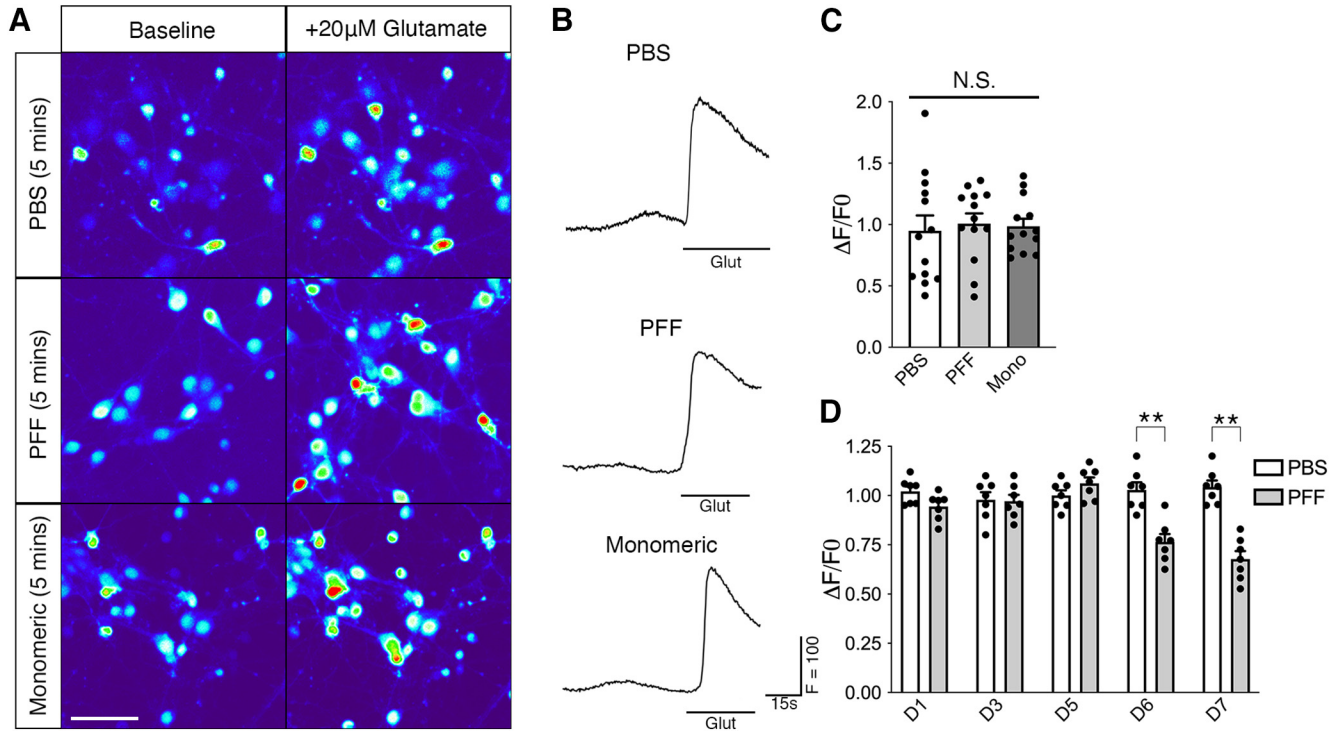

Figure 3. PFF induced inhibition of glutamate-evoked calcium influx manifests over several days. ***A–C***, Heatmap of representative micrographs depicts Fluo-4 AM fluorescence intensity in cortical neurons before and after stimulation with 20 μM glutamate (***A***). Representative traces of calcium transients show no change in calcium influx in response to 20 μM glutamate in neurons immediately after PFF exposure (***B***). Quantification of average intracellular glutamate-evoked calcium flux shows no change in PFF-exposed neurons relative to PBS and monomeric α-syn controls (***C***). Data are mean + SEM. N.S., Not significant (ANOVA with *post hoc* Tukey); $n = 13$ or 14 replicate experiments. ***D***, Quantification of average intracellular glutamate-evoked calcium flux at 24 h intervals after PFF exposure shows a significant decrease in PFF-exposed neurons relative to PBS and monomeric α-syn controls at 6 d after PFF exposure and beyond. Data are mean + SEM. $^{**}p < 0.01$ (two-way ANOVA with *post hoc* Sidak's test); $n = 7$ independent experiments.

(Hayashi and Majewska, 2005). Moreover, monomeric α-syn exposure led to an increase in proximal stubby spines (Fig. 5*B*) within 5 d of exposure. These are predominant in early synapse formation and may be indicative monomeric α-syn induced changes in spine dynamics (Hering and Sheng, 2001). Collectively, these data suggest that the accumulation of α-syn pathology in synaptic regions leads to impaired NMDAR activation coupled with the loss of mature synaptic connections.

PFF exposure promotes NO accumulation and S-nitrosylation of MAP1A

To establish a mechanistic link between α-syn pathology and loss of synaptic function, we tested whether the kinetics of NO synthesis were altered by intracellular α-syn aggregation. α-Syn-PFF treatment has been previously reported to increase NO levels in primary cortical neurons (Kam et al., 2018). We therefore asked whether increased NO may relate to the observed deficits in cortico-synaptic function. Neurons were exposed to PFFs for 24 h, coincident with the first observation of intracellular accumulation of multimeric α-syn. We then loaded cells with the NO-reactive dye DAF-FM and measured the kinetics of NO accumulation over a 30 min period. The rate of NO synthesis was far greater in PFF exposure neurons than in vehicle control (Fig. 6*A–C*). This effect was specifically observed in neuritic extensions (Fig. 6*A*, arrows). To determine whether increased kinetics of NO synthesis results in synaptic dysfunction following PFF exposure, we sought to determine whether any member of the NMDAR complex, or any known protein binding partner that has been ascribed a role in regulating NMDAR function, was specifically modified by NO. NO-related species can react with critical cysteine residues to affect functional activity of many proteins via protein S-nitrosylation (forming SNO proteins) (Stamler et al., 1992; Lipton et al., 1993). Using Genemania, we performed a bioinformatic screen of known NMDAR subunit protein interactors. We identified 21 known protein interactors of the 6 major NMDAR subunits (GRIN1, GRIN2A, GRIN2B, GRIN2C, GRIN3A, GRIN3B). We then contrasted this list against published SNO-proteomic datasets (Hao et al., 2006; Doulias et al., 2013; Zahid et al., 2014; Zaręba-Kozioł et al., 2014; Seneviratne et al., 2016; Mnatsakanyan et al., 2019) that evaluated S-nitrosylation of proteins in samples of neural origin (Extended Data Fig. 6-1). This analysis identified four proteins critical to the function of the NMDAR complex that are SNO-modified in various physiological settings (DYNLL2, GRIN1, GRIN2B, and MAP1A) (Fig. 6*D*; Extended Data Fig. 6-1). We next sought to determine whether any of the identified protein-candidates were SNO-modified in response to PFF exposure. Using the biotin switch method to label SNO-modified cysteines with biotin for subsequent capture, we exposed neural cells to PFFs or α-syn monomers to determine whether DYNLL2, GRIN1, GRIN2B, and MAP1A were S-nitrosylated 7 d after exposure. The physiological NO-donor S-nitrosocysteine was used as a control for the ability of each protein to be nitrosylated in this system. Silver stain of biotin labeled proteins showed increase SNO proteins in cells 7 d after exposure to PFFs, relative to monomeric α-syn (Fig. 6*E*). Following subsequent biotin capture, only MAP1A was found to be S-nitrosylated in response to PFF exposure. The observed increase in SNO-MAP1A following exposure to PFFs was reversed by 24 h treatment with the NO synthase (NOS) inhibitor L-NAME (Fig. 6*F*), while the detection of SNO-MAP1A was completely abolished in

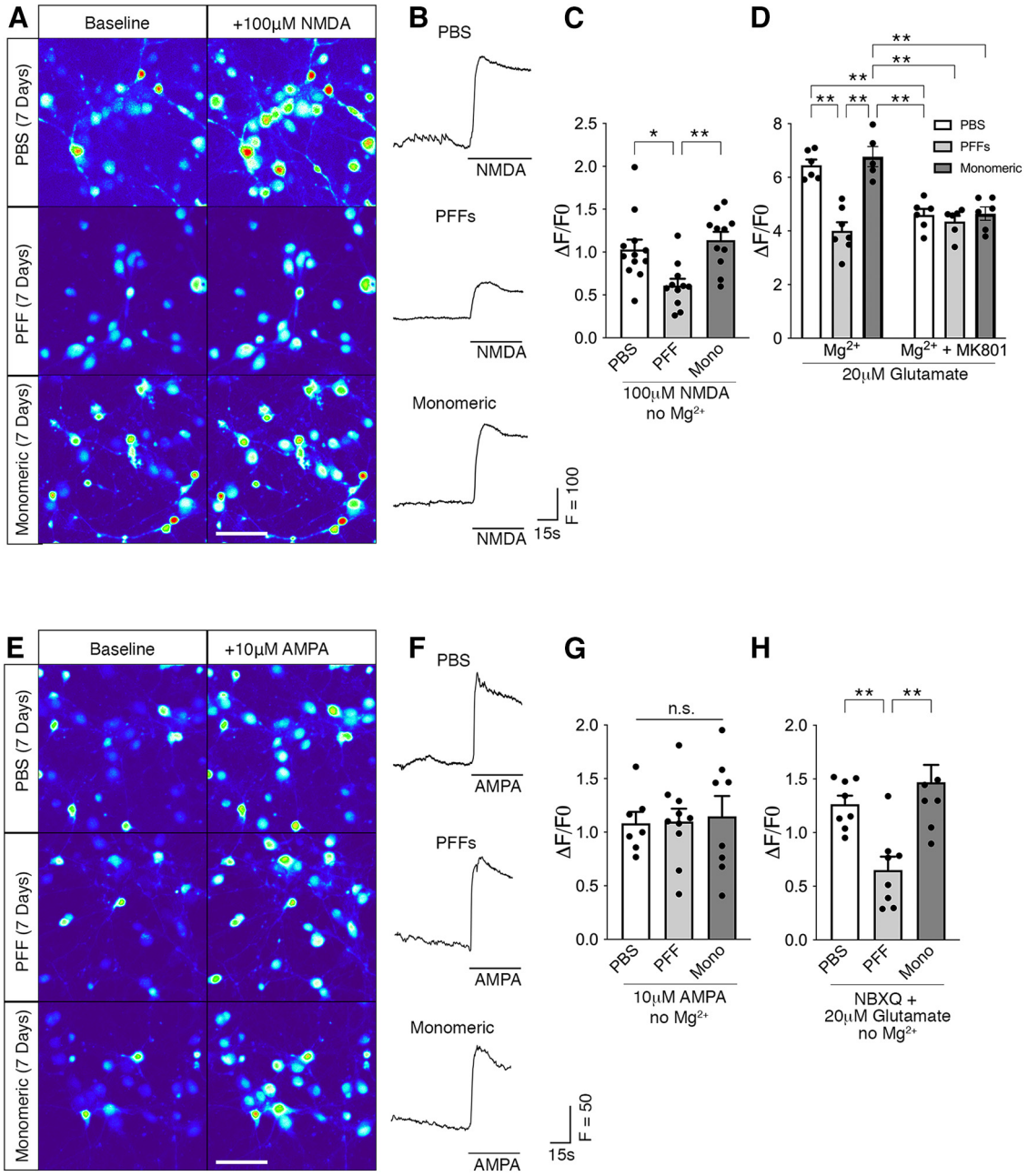

Figure 4. PFF exposure impairs calcium influx via NMDARs. ***A–C***, Heatmap of representative micrographs depicts Fluo-4 AM fluorescence intensity in cortical neurons before and after stimulation with 100 μM NMDA in the absence of Mg^{2+} (***A***). Representative traces of calcium transients show reduced calcium influx in response to 100 μM NMDA in the absence of Mg^{2+} in neurons 7 d after PFF exposure (***B***). Quantification of average intracellular NMDA-evoked calcium flux shows a significant decrease in PFF-exposed neurons relative to PBS and monomeric α-syn controls (***C***). Data are mean + SEM. *$p < 0.05$; **$p < 0.01$; ANOVA with *post hoc* Tukey; $n = 11$ or 12 replicate experiments. ***D***, Quantification of intracellular calcium flux in primary cortical neurons in response to glutamate with and without a 30 min preblock with 10 μM MK-801 by live-cell Fluo-4 AM imaging. Data are mean + SEM. **$p < 0.01$ (two-way ANOVA with *post hoc* Sidak's test); $n = 7$ independent experiments. ***E–G***, Heatmap of representative micrographs depicts Fluo-4 AM fluorescence intensity in cortical neurons before and after stimulation with 10 μM AMPA in the absence of Mg^{2+} (***E***). Representative traces of calcium transients show no change in calcium influx in response to 10 μM AMPA in the absence of Mg^{2+} in neurons 7 d after PFF exposure (***F***). Quantification of average intracellular AMPA-evoked calcium flux shows no change in PFF-exposed neurons relative to PBS and monomeric α-syn controls (***G***). Data are mean + SEM. n.s., Not significant (ANOVA with *post hoc* Tukey); $n = 7$-10 independent experiments. ***H***, Quantification of intracellular calcium flux in response to glutamate following 30 min preblocking with AMPA-specific antagonist NBQX. Data are mean + SEM. **$p < 0.01$ (ANOVA with *post hoc* Tukey); $n = 8$ replicate experiments.

the absence of ascorbate reduction (Fig. 6*G*), confirming that the increase in SNO-MAP1A was a specific response to PFF-induced NOS activity.

Preventing NO generation rescues PFF-evoked synaptic deficits

To determine whether blocking NO synthesis, and subsequent S-nitrosylation of MAP1A, normalized the synaptic deficits evoked by PFF exposure, we treated cortical neurons with L-NAME for 24 h, 6 d after PFF exposure. This timing was chosen to coincide with the first observed deficit in glutamate evoke response (Fig. 3*D*). L-NAME treatment rescued PFF-evoked loss of mature (mushroom) spines in both the proximal (Fig. 7*A*) and distal (Fig. 7*B*) dendritic regions. Interestingly, L-NAME also seemed to alter the effect of monomeric α-syn on spine dynamics, increasing the number of thin spines observed in distal dendrites

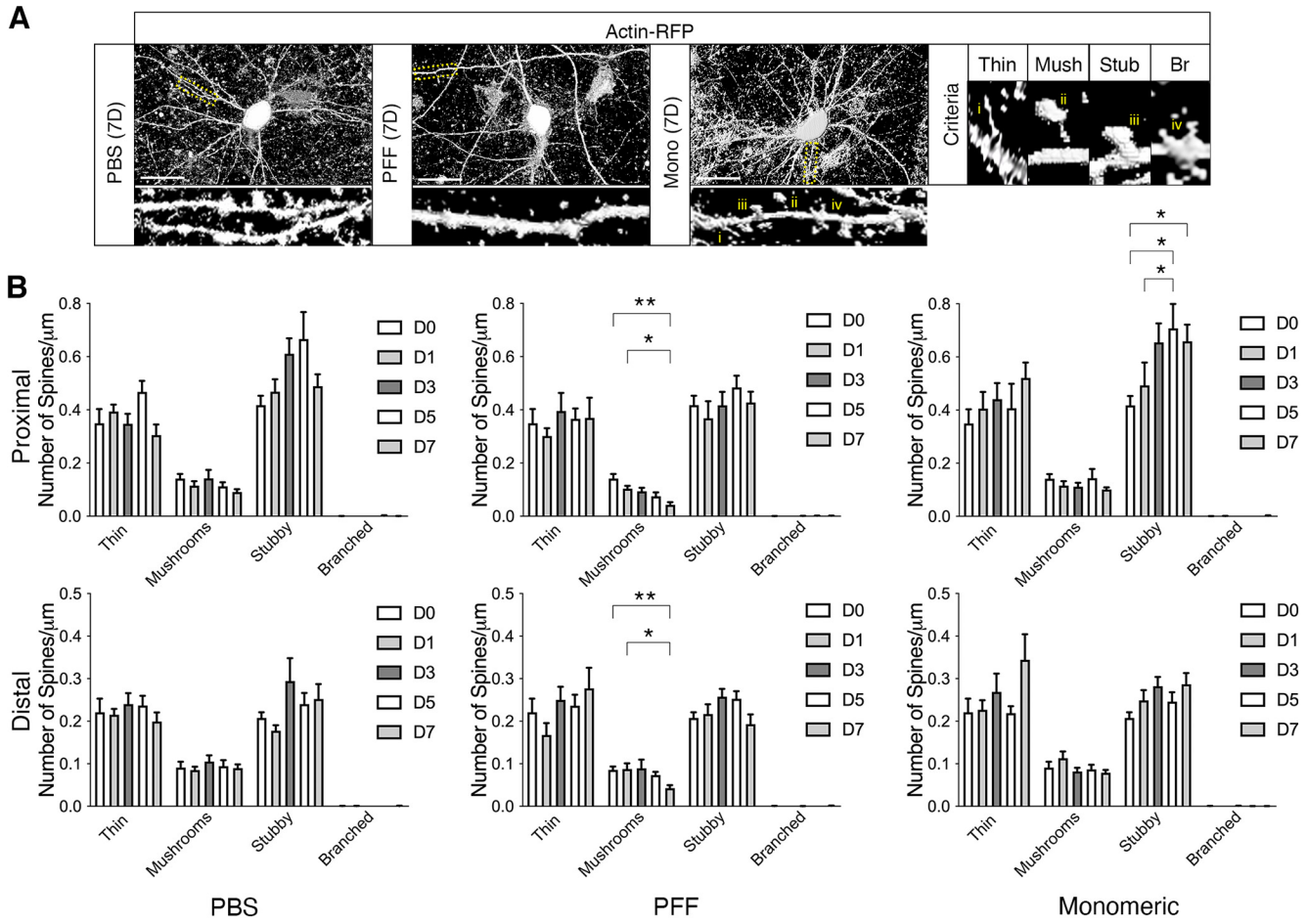

Figure 5. PFF exposure results in loss of mature spines. ***A***, Neurons were transformed with LifeAct(Actin)-RFP before exposure to PBS, α-syn monomer, or α-syn PFFs. Post exposure, cells were fixed and imaged to assess morphology of dendritic spines. Scale bar, 10 μm. Spines were characterized as Thin (i), Mushroom (Mush, ii), Stubby (Stub, iii), or Branched (Br, iv) based on their 3D morphology. ***B***, Quantification spines of each morphologic type that resided >60 μm from the soma (Distal) or that resided <60 μm from the soma (Proximal). Data are mean + SEM. *$p < 0.05$; **$p < 0.01$; two-way ANOVA with *post hoc* Sidak's test; $n = 9$ independent experiments.

exposed to α-syn monomers. Moreover, L-NAME treatment abolished PFF-induced deficits in glutamate-evoked calcium influx (Fig. 7*C–E*). Collectively, these findings strongly suggest that accumulation of intracellular α-syn aggregates triggers synaptic dysfunction in an NO-dependent manner. In our final set of experiments, we sought to evaluate whether lowering the steady-state levels of NO restored network activity in PFF-exposed cortical cultures. Primary cortical neurons were seeded onto MEA plates and treated with L-NAME or vehicle for 24 h 6 d after PFF or monomeric α-syn exposure and spontaneous activity was recorded (Fig. 8*A*). We then quantitatively assessed the mean firing rate, bursting activity, and synchrony index across all conditions (Fig. 8*B–D*). We found that PFF exposure significantly inhibited all network activity parameters and that treatment with L-NAME significantly rescued these deficits (Fig. 8)*B–D*. These data collectively suggest that, by normalizing glutamate-evoked NMDAR activation, L-NAME restores the deficits in cortical network activity induced by intracellular α-syn aggregates. We therefore propose a model in which, intercellular α-syn oligomer binding-coincident with deposition of intracellular α-syn aggregates stimulates NO synthesis through nNOS (Fig. 9*A*,*B*). The increase in dendritic NO-related species leads to S-nitrosylation of MAP1A and the destabilization of mature dendritic spines, resulting in inhibition of glutamate-evoked NMDAR responses and impairments in cortical network activity (Fig. 9*C*). NO-mediated post-translational modification to synaptic proteins may consequently represent a critical mediator of cortical dysfunction in synucleinopathies.

Discussion

In the current study, we demonstrated that intracellular accumulation of α-syn pathology results in increased NO synthesis and S-nitrosylation of the MAP1A scaffold protein. This in turn led to inhibition of NMDAR activity and loss of dendritic spines. Excess NO has been implicated in multiple aspects of PD pathogenesis. Postmortem analysis of midbrain samples from PD patients has revealed that nNOS expression is increased in this brain region relative to controls (Eve et al., 1998). nNOS activity is also upregulated in MPTP rodent models of PD (Watanabe et al., 2008; Joniec et al., 2009). Elevated levels of inducible NOS (iNOS), by contrast, have been found in postmortem brain samples from multiple brain regions of persons with Parkinsonian disorders (Hunot et al., 1996). In support of this observation, there is also increased iNOS expression in multiple animal models of PD, including 6-OHDA (Broom et al., 2011), MPTP (Zhu et al., 2020), and α-syn-oligomer evoked models (Tapias et al., 2017), whereas mice lacking iNOS are resistant to many toxin-evoked PD-inducing paradigms (Dehmer et al., 2000). nNOS contains a PDZ domain that confers binding capacity to many

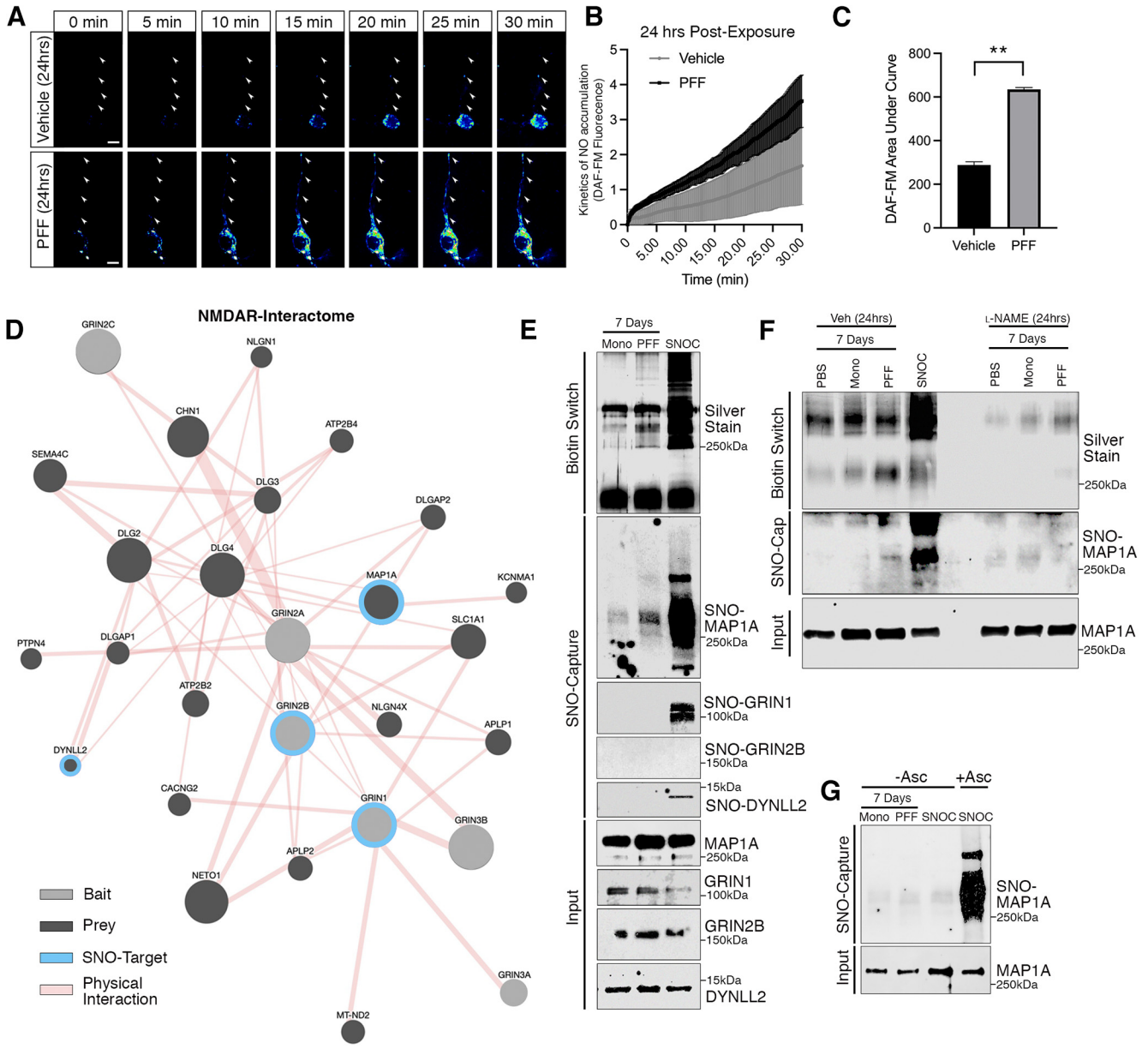

Figure 6. PFF exposure promotes NO accumulation and S-nitrosylation of MAP1A. ***A–C***, Neurons were exposed to PFFs for 24 h before DAF-FM live imaging. Micrographs represent a heat-map of DAF-FM reactivity (***A***). Arrows indicate DAF-FM reactivity specifically in neuritic extensions. Kinetics of NO accumulation were quantified over a 30 min period (***B***), showing that NO synthesis was significantly increased in PFF exposure neurons than in vehicle control (***C***). Data are mean ± SEM. $^{**}p < 0.01$ (*t* test of area under the curve). ***D***, Prediction of NMDAR subunit protein interactors generated using Genemania identified 21 known protein interactors (dark gray represents prey) of the six major NMDAR subunits (light gray represents bait). When cross-referenced against published SNO-proteomic datasets that evaluated S-nitrosylation of proteins in samples of neural origin (see Extended Data Fig. 6-1), four proteins known to be SNO-modified (light blue). ***E***, Neural cells (SH-SY5Y) were analyzed by biotin switch (silver stain) 7 d after exposure to PFFs or α-syn monomers, or 5 min exposure to S-nitrosocysteine. Following biotin labeling, SNO proteins were captured with Neutravidin and lysates probed for MAP1A, GRIN1, GRIN2B, or DYNLL2. Only MAP1A was found to be S-nitrosylated in response to PFF exposure. ***F***, Biotin switch-capture in the presence of L-NAME reversed of SNO modification of MAP1A. ***G***, Biotin switch in the absence of ascorbate reduction abolished SNO-MAP1A.

postsynaptic density proteins (including PSD93 and PSD95) and is therefore regionally distributed along synaptic spines (Brenman et al., 1996). This localization is key to its canonical role in promoting NO-mediated second messenger signaling. The guanylate kinase domain of PSD-95 directly binds to the GMP-binding sequence in the C-terminus of MAP1A (Reese et al., 2007), whereas the second PDZ domain of PSD-95 binds to the seven-amino acid C-terminal domain of NMDAR, common to NR2 subunits and certain NR1 splice forms (Kornau et al., 1995). Thus, these proteins resolve into a single complex that is a master effector of NMDAR signal transduction. Map1a KO mice exhibit NMDAR-dependent learning disabilities, characterized by reduced EPSCs and a concomitant decrease in LTP and LTD (Takei et al., 2015), supporting the notion that MAP1A is an effector of NMDAR signaling. Moreover, targeted deletion of the Map1a gene leads to abnormal focal swellings of dendritic shafts and disruptions in axon initial segment morphology, leading to neurodegeneration (Liu et al., 2015). Loss of synaptic localization of NR2A and NR2B subunits are suggested to be responsible for altered synaptic function in neurons lacking MAP1A (Takei et al., 2015). These data suggest that tethering of NMDARs to the cytoskeleton through MAP1A is fundamental for receptor localization and function. Indeed, the conserved C-terminal MAP1 homology

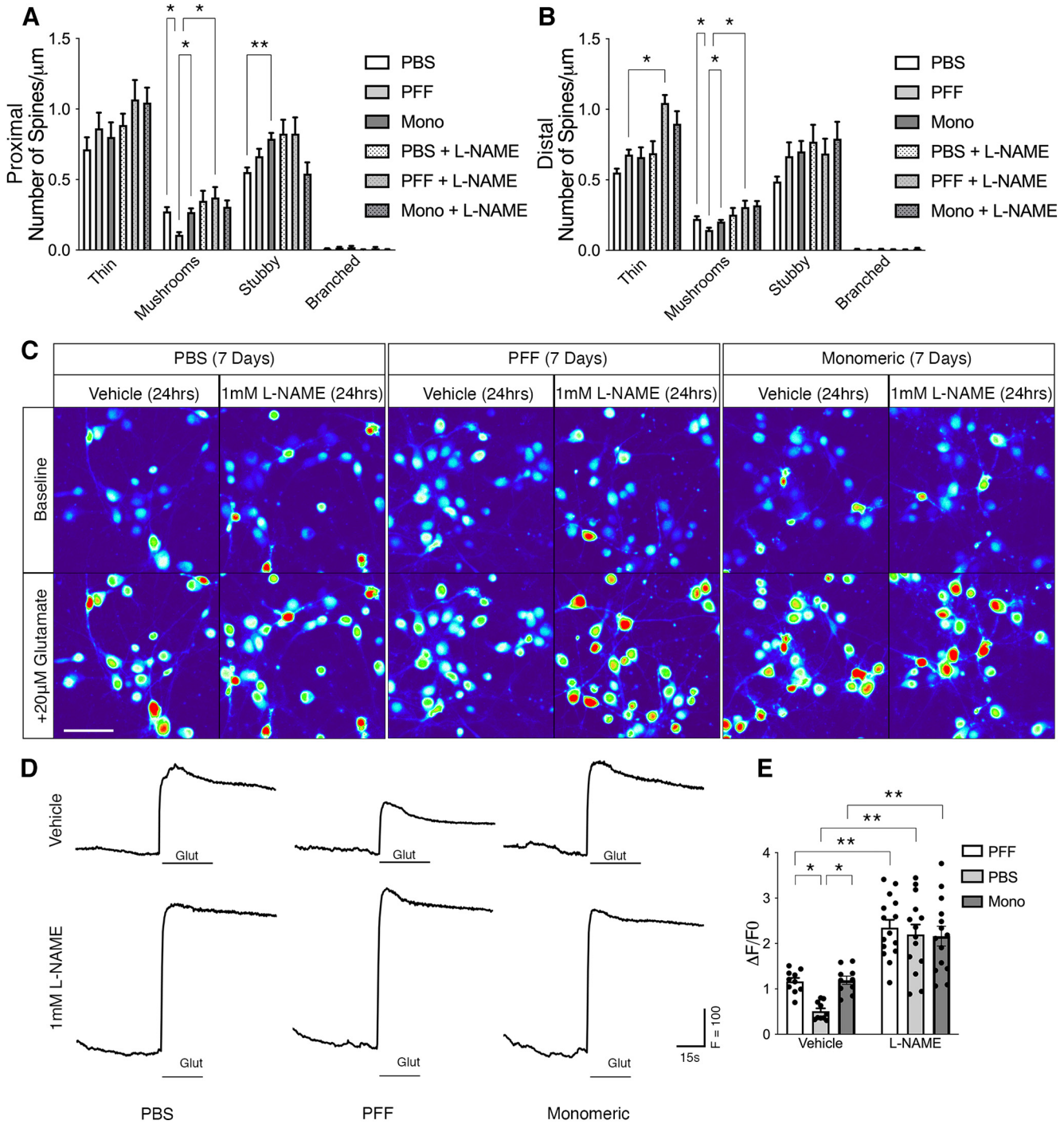

Figure 7. L-NAME rescues PFF-induced deficits in glutamate response and spine morphology. ***A***, ***B***, Quantification of spines of each morphologic type (characterized as Thin, Mushroom [Mush], Stubby [Stub], or Branched [Br]) that resided <60 µm from the soma (proximal) (***A***) or >60 µm from the soma (distal) (***B***). Data are mean + SEM. $*p < 0.05$; $**p < 0.01$; two-way ANOVA with *post hoc* Sidak's test; $n = 9$ independent experiments. ***C–E***, Heatmap of representative micrographs represent Fluo-4 AM fluorescence intensity in cortical neurons 7 d after PBS, PFF, or monomeric α-syn exposure. Neurons were treated with 1 mM L-NAME before stimulation with 20 µM glutamate. Pictures represent before and after stimulation (***C***). Representative traces of calcium transients show L-NAME rescued calcium influx in response to 20 µM glutamate in neurons 7 d after PFF exposure (***D***). Quantification of average intracellular glutamate-evoked calcium flux in PFF-exposed neurons relative to PBS and monomeric α-syn controls, with and without L-NAME (***E***). Data are mean + SEM. $*p < 0.05$; $**p < 0.01$; two-way ANOVA with *post hoc* Sidak's test; $n = 10$-14 independent experiments.

domain present in all MAP1 family members has been shown to bind the intracellular C-terminus of human NR3A and NR1 directly (Eriksson et al., 2007), thus supporting our observations that MAP1A is critical for stabilizing NMDAR function.

The effect of α-syn on NMDAR function seems dependent, in part, on the brain region studied. In the hippocampus, exposure to aggregated α-syn seems to increase NMDAR activity. For instance, exposure of hippocampal neurons to α-syn oligomers for 90 min increases basal synaptic transmission through NMDAR activation, coupled to enhanced signaling through calcium-permeable AMPARs (Diogenes et al., 2012). Similarly, acute exposure to extracellular α-syn-PFFs is reported to increase astrocytic release of glutamate in the hippocampus while increasing extrasynaptic NMDAR and AMPAR activity (Trudler et al.,

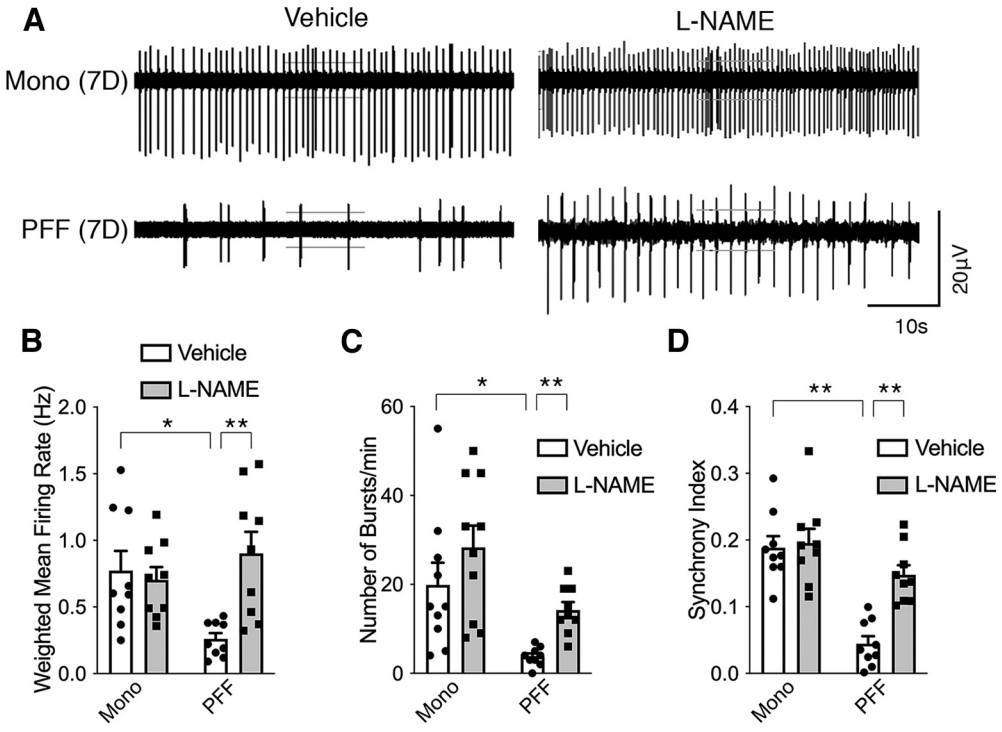

Figure 8. L-NAME rescues PFF-induced deficits in neuronal network activity. ***A***, Representative continuous waveform plots recorded from cortical neurons 7 d after exposure to PFFs or monomeric α-syn. Twenty-four hours before recording, cells were treated with 1 mM L-NAME 1 or vehicle. Spontaneous neuronal spiking is observed when the electrical signal exceeds the electrode's noise threshold (cross bars) measured by multielectrode array. ***B–D***, Quantification of neural metrics recorded by multielectrode array for 10 min in culture medium at 37°C. The weighted mean firing rate (***B***) and average number of bursts (***C***) for each independent well were used to calculate the mean and SEM for each condition. Average synchrony index (***D***) is shown as a measure of the degree of synaptic connectivity in each condition. Data are mean + SEM. $^{**}p < 0.01$ (two-way ANOVA with *post hoc* Tukey's test); $n = 9$ independent experiments.

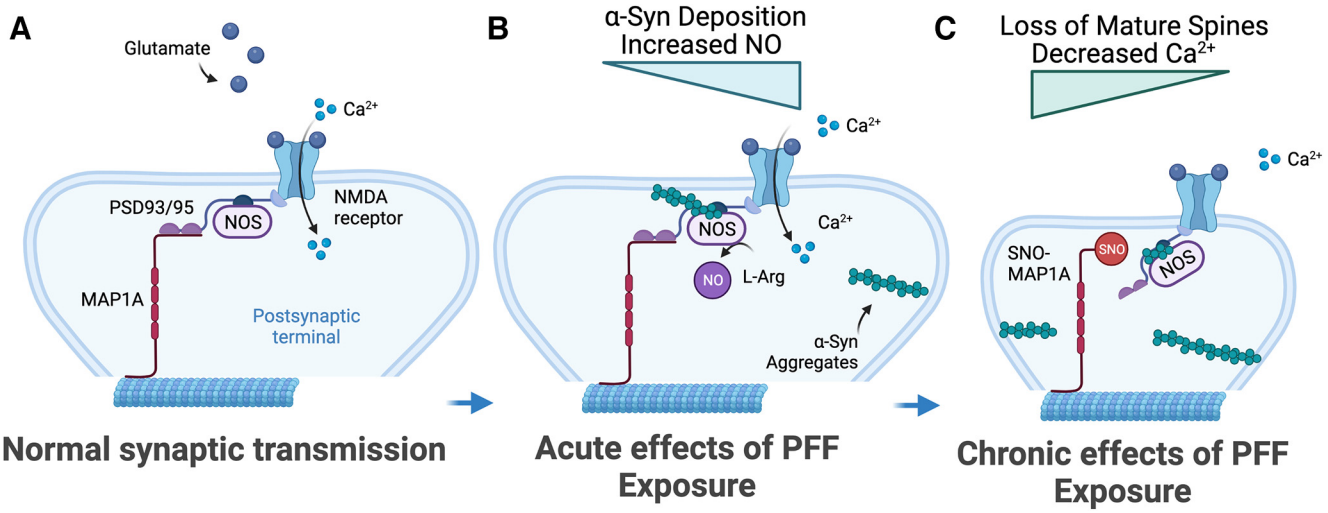

Figure 9. Model of PFF-evoked synaptic dysfunction. ***A–C***, Healthy neuron depicted (***A***). Intercellular α-syn oligomer binding-coincident with deposition of intracellular aggregates stimulates NO synthesis through nNOS (***B***). The increase in dendritic NO leads to S-nitrosylation of MAP1A and the destabilization of mature dendritic spines, resulting in inhibition of glutamate-evoked NMDAR responses and impairments in cortical network activity (***C***). Schematic was generated using www.BioRender.com.

2021). In cortical regions, by contrast, incubation of corticostriatal slice cultures for 1 h with α-syn oligomers was shown to reduce NMDAR-mediated synaptic currents and impair LTP through physical interaction with NR2A subunits (Durante et al., 2019). This is consistent with reports from prolonged PFF exposure that have been associated with impairments in neuronal excitability and connectivity in primary cortical neurons, wherein decreased synaptic function was associated with decreased numbers of mature (mushroom) spines (Volpicelli-Daley et al., 2011). Seemingly paradoxically, the same group demonstrated in a follow-up study that hippocampal neurons exhibit the opposite effect to that seen in cortical neurons (i.e., an increase in mEPSCs frequency rather than a decrease) when exposed to PFFs for 7 d. This was nonetheless accompanied by a reduction in postsynaptic spine density (Froula et al., 2018). The authors went on to show that the reduction in spine density occurred only in WT primary neurons exposed to PFFs and not in neurons from SNCA-KO mice exposed to PFFs, suggesting that the changes in

spine morphology result from fibril-induced corruption of endogenously expressed α-syn (Froula et al., 2018). The deposition of α-syn inclusions following *in vivo* PFF inoculation has also been shown to occur only in WT animals and not in SNCA-KO animals inoculated with PFFs, further supporting that loss of synaptic function is a consequence of α-syn aggregation. Indeed, long-term *in vivo* imaging of apical dendrites performed in mice overexpressing WT human α-synuclein coupled with intracranial injection of preformed α-synuclein fibrils both show decreased spine density and abnormalities in spine dynamics (i.e., loss of mushroom spines) in an age-dependent manner (Blumenstock et al., 2017). We therefore propose a model in which the effects of α-syn-PFFs on NMDAR activity are a function both the kinetics of fibrilization and subcellular localization (Fig. 9). Low concentration of extracellular α-syn micro-aggregates may increase iGluR activity that is associated with increased nNOS activation and NO synthesis. As these micro-aggregates are internalized and seed further intracellular α-syn aggregation, the subsequent increase in RNS acts to deactivate the NMDAR complex and reduce further calcium influx, creating a negative feedback loop. The accumulation of α-syn inclusions at the postsynaptic terminus coupled to elevated NO levels alters the stability of mature synaptic spines, in part, although S-nitrosylation of the synaptic scaffold protein MAP1A.

In contrast to the effect of α-syn fibrilization after PFF exposure, we also find that prolonged monomer exposure has a modest impact on synaptic spine morphology in association with increased soluble α-syn-PS129 levels. These effects are likely independent of α-syn fibrilization as PS129 labeling is known to occur on soluble, nonaggregated, or membrane-associated protein (Nuber et al., 2018; Imberdis et al., 2019), and we observe no deposition of insoluble α-syn or aggregated α-syn accumulation following monomer exposure. Thus, the effects of monomer exposure are likely because of α-syn protein accumulation and PS129 post-translational modification and not α-syn fibrilization per se. It may therefore stand to reason that nitrosative stress is a specific consequence of the fibrilization event.

A number of aberrantly S-nitrosylated proteins have been implicated in neurodegenerative disorders and may contribute to specific disease pathology (Nakamura et al., 2013). In support of this notion in PD, gene ontology clustering after genetic profiling of patient-derived PD neurons relative to control neurons showed aberrations in biological processes related to metabolism of nitrogen-containing compounds (Ryan et al., 2013; Czaniecki et al., 2019). We show that blocking NO synthesis via L-NAME prevents MAP1A S-nitrosylation and normalizes synaptic function. While not subject to S-nitrosylation, given the absence of cysteine residues, tyrosine nitration of α-syn can potentiate α-syn-oligomer formation. Exposure of α-syn to NO can encourage o,o′-dityrosine crosslinking between the N-terminal and C-terminal tyrosines to generate α-syn-dimers that enhance oligomer deposition (Krishnan et al., 2003; Hodara et al., 2004; Danielson et al., 2009; Burai et al., 2015). Additionally, tyrosines play an important role in α-syn-vesicle binding, whereas nitration impairs this interaction by altering the charge at the N-terminal domain and/or causing a conformational change at the C-terminal domain. By decreasing the amount of α-syn present in a vesicle bound α-helical conformation, oligomer formation is thereby potentiated (Hodara et al., 2004; Sevcsik et al., 2011; Burai et al., 2015). The observed accumulation of NO in PFF-exposed neurons and the propensity of nitrated α-syn to promote the seeding of α-syn pathology (Musgrove et al., 2019) may explain why we see the accumulation of PS129-modifed α-syn at synaptic terminals.

Evidence suggests that nitration of α-syn can also potentiate fibril formation. In cells exposed to peroxynitrite, aggregation of α-syn is dependent on nitro-tyrosine adduct formation (Paxinou et al., 2001). Indeed, nitrated α-syn is almost exclusively found in the insoluble protein fraction, making it more resistant to degradation, more compact, and more stable (Norris et al., 2003; Uversky et al., 2005). It is therefore interesting to speculate as to whether NO-modified proteins may serve as markers for prognostication in PD or Lewy body dementia. That NO-modified proteins of multiple types represent viable clinical targets in synucleinopathies is supported by recent clinical trials using N-acetylcysteine (NAC). NAC represents a stable reduced form of cysteine that, on cleavage of the acetyl group, reveals reduced Cys, which is available for incorporation into the highly abundant intracellular antioxidant, glutathione (Rushworth and Megson, 2014). Glutathione in turn has a major role in antioxidant protection to protein thiolation and can specifically reduce S-nitrosylation, among other thiol oxidation types (Lipton et al., 1993; Clementi et al., 1998). Clinical evaluation has shown that NAC increases dopamine levels with a concomitant improvement in the Universal Parkinson's Disease Rating Scale total scores in patients with PD receiving intravenous NAC supplemented by oral NAC between infusions (Holmay et al., 2013; Monti et al., 2019). Moreover, both the motor and nonmotor subcomponents of the Universal Parkinson's Disease Rating Scale showed improvement. Collectively, this work suggests that SNO-cysteine thiols may be viable targets against synaptic dysfunction in multiple synucleinopathies. Thus, reducing or controlling RNS accumulation early in disease etiology may have multimodal benefits to people with Lewy body dementia.

References

Bello-Medina PC, Flores G, Quirarte GL, McGaugh JL, Prado Alcala RA (2016) Mushroom spine dynamics in medium spiny neurons of dorsal striatum associated with memory of moderate and intense training. Proc Natl Acad Sci USA 113:E6516–E6525.

Blumenstock S, Rodrigues EF, Peters F, Blazquez-Llorca L, Schmidt F, Giese A, Herms J (2017) Seeding and transgenic overexpression of alpha-synuclein triggers dendritic spine pathology in the neocortex. EMBO Mol Med 9:716–731.

Brenman JE, Chao DS, Gee SH, McGee AW, Craven SE, Santillano DR, Wu Z, Huang F, Xia H, Peters MF, Froehner SC, Bredt DS (1996) Interaction of nitric oxide synthase with the postsynaptic density protein PSD-95 and alpha1-syntrophin mediated by PDZ domains. Cell 84:757–767.

Broom L, Marinova-Mutafchieva L, Sadeghian M, Davis JB, Medhurst AD, Dexter DT (2011) Neuroprotection by the selective iNOS inhibitor GW274150 in a model of Parkinson disease. Free Radic Biol Med 50:633–640.

Burai R, Ait-Bouziad N, Chiki A, Lashuel HA (2015) Elucidating the role of site-specific nitration of alpha-synuclein in the pathogenesis of Parkinson's disease via protein semisynthesis and mutagenesis. J Am Chem Soc 137:5041–5052.

Chen Y, Yang W, Li X, Li X, Yang H, Xu Z, Yu S (2015) alpha-Synuclein-induced internalization of NMDA receptors in hippocampal neurons is associated with reduced inward current and Ca(2+) influx upon NMDA stimulation. Neuroscience 300:297–306.

Chicurel ME, Harris KM (1992) Three-dimensional analysis of the structure and composition of CA3 branched dendritic spines and their synaptic relationships with mossy fiber boutons in the rat hippocampus. J Comp Neurol 325:169–182.

Choi YB, Lipton SA (2000) Redox modulation of the NMDA receptor. Cell Mol Life Sci 57:1535–1541.

Clementi E, Brown GC, Feelisch M, Moncada S (1998) Persistent inhibition of cell respiration by nitric oxide: crucial role of S-nitrosylation of mitochondrial complex I and protective action of glutathione. Proc Natl Acad Sci USA 95:7631–7636.

Colom-Cadena M, et al. (2017) Synaptic phosphorylated alpha-synuclein in dementia with Lewy bodies. Brain 140:3204–3214.

Cooper AA, Gitler AD, Cashikar A, Haynes CM, Hill KJ, Bhullar B, Liu K, Xu K, Strathearn KE, Liu F, Cao S, Caldwell KA, Caldwell GA, Marsischky G, Kolodner RD, Labaer J, Rochet JC, Bonini NM, Lindquist S (2006) Alpha-synuclein blocks ER-Golgi traffic and Rab1 rescues neuron loss in Parkinson's models. Science 313:324–328.

Czaniecki C, Ryan T, Stykel MG, Drolet J, Heide J, Hallam R, Wood S, Coackley C, Sherriff K, Bailey CD, Ryan SD (2019) Axonal pathology in hPSC-based models of Parkinson's disease results from loss of Nrf2 transcriptional activity at the Map1b gene locus. Proc Natl Acad Sci USA 116:14280–14289.

Danielson SR, Held JM, Schilling B, Oo M, Gibson BW, Andersen JK (2009) Preferentially increased nitration of alpha-synuclein at tyrosine-39 in a cellular oxidative model of Parkinson's disease. Anal Chem 81:7823–7828.

Dehmer T, Lindenau J, Haid S, Dichgans J, Schulz JB (2000) Deficiency of inducible nitric oxide synthase protects against MPTP toxicity in vivo. J Neurochem 74:2213–2216.

Dikic I (2017) Proteasomal and autophagic degradation systems. Annu Rev Biochem 86:193–224.

Diogenes MJ, Dias RB, Rombo DM, Vicente Miranda H, Maiolino F, Guerreiro P, Nasstrom T, Franquelim HG, Oliveira LM, Castanho MA, Lannfelt L, Bergstrom J, Ingelsson M, Quintas A, Sebastiao AM, Lopes LV, Outeiro TF (2012) Extracellular alpha-synuclein oligomers modulate synaptic transmission and impair LTP via NMDA-receptor activation. J Neurosci 32:11750–11762.

Doulias PT, Tenopoulou M, Greene JL, Raju K, Ischiropoulos H (2013) Nitric oxide regulates mitochondrial fatty acid metabolism through reversible protein s-nitrosylation. Sci Signal 6:rs1.

Durante V, et al. (2019) Alpha-synuclein targets GluN2A NMDA receptor subunit causing striatal synaptic dysfunction and visuospatial memory alteration. Brain 142:1365–1385.

Emanuele M, Esposito A, Camerini S, Antonucci F, Ferrara S, Seghezza S, Catelani T, Crescenzi M, Marotta R, Canale C, Matteoli M, Menna E, Chieregatti E (2016) Exogenous alpha-synuclein alters pre- and post-synaptic activity by fragmenting lipid rafts. EBioMedicine 7:191–204.

Eriksson M, Samuelsson H, Samuelsson EB, Liu L, McKeehan WL, Benedikz E, Sundstrom E (2007) The NMDAR subunit NR3A interacts with microtubule-associated protein 1S in the brain. Biochem Biophys Res Commun 361:127–132.

Eve DJ, Nisbet AP, Kingsbury AE, Hewson EL, Daniel SE, Lees A, Marsden CD, Foster OJ (1998) Basal ganglia neuronal nitric oxide synthase mRNA expression in Parkinson's disease. Brain Res Mol Brain Res 63:62–71.

Fortin DL, Troyer MD, Nakamura K, Kubo S, Anthony MD, Edwards RH (2004) Lipid rafts mediate the synaptic localization of alpha-synuclein. J Neurosci 24:6715–6723.

Froula JM, Henderson BW, Gonzalez JC, Vaden JH, McLean JW, Wu Y, Banumurthy G, Overstreet-Wadiche L, Herskowitz JH, Volpicelli-Daley LA (2018) alpha-Synuclein fibril-induced paradoxical structural and functional defects in hippocampal neurons. Acta Neuropathol Commun 6:35.

Garthwaite J, Charles SL, Chess-Williams R (1988) Endothelium-derived relaxing factor release on activation of NMDA receptors suggests role as intercellular messenger in the brain. Nature 336:385–388.

Hao G, Derakhshan B, Shi L, Campagne F, Gross SS (2006) SNOSID, a proteomic method for identification of cysteine S-nitrosylation sites in complex protein mixtures. Proc Natl Acad Sci USA 103:1012–1017.

Hardingham N, Fox K (2006) The role of nitric oxide and GluR1 in presynaptic and postsynaptic components of neocortical potentiation. J Neurosci 26:7395–7404.

Harris KM, Jensen FE, Tsao B (1992) Three-dimensional structure of dendritic spines and synapses in rat hippocampus (CA1) at postnatal day 15 and adult ages: implications for the maturation of synaptic physiology and long-term potentiation. J Neurosci 12:2685–2705.

Hayashi Y, Majewska AK (2005) Dendritic spine geometry: functional implication and regulation. Neuron 46:529–532.

Hering H, Sheng M (2001) Dendritic spines: structure, dynamics and regulation. Nat Rev Neurosci 2:880–888.

Hodara R, Norris EH, Giasson BI, Mishizen-Eberz AJ, Lynch DR, Lee VM, Ischiropoulos H (2004) Functional consequences of alpha-synuclein tyrosine nitration: diminished binding to lipid vesicles and increased fibril formation. J Biol Chem 279:47746–47753.

Holmay MJ, Terpstra M, Coles LD, Mishra U, Ahlskog M, Oz G, Cloyd JC, Tuite PJ (2013) N-Acetylcysteine boosts brain and blood glutathione in Gaucher and Parkinson diseases. Clin Neuropharmacol 36:103–106.

Hunot S, Boissiere F, Faucheux B, Brugg B, Mouatt-Prigent A, Agid Y, Hirsch EC (1996) Nitric oxide synthase and neuronal vulnerability in Parkinson's disease. Neuroscience 72:355–363.

Imberdis T, Negri J, Ramalingam N, Terry-Kantor E, Ho GP, Fanning S, Stirtz G, Kim TE, Levy OA, Young-Pearse TL, Selkoe D, Dettmer U (2019) Cell models of lipid-rich alpha-synuclein aggregation validate known modifiers of alpha-synuclein biology and identify stearoyl-CoA desaturase. Proc Natl Acad Sci USA 116:20760–20769.

Iwai A, Masliah E, Yoshimoto M, Ge N, Flanagan L, de Silva HA, Kittel A, Saitoh T (1995) The precursor protein of non-A beta component of Alzheimer's disease amyloid is a presynaptic protein of the central nervous system. Neuron 14:467–475.

Joniec I, Ciesielska A, Kurkowska-Jastrzebska I, Przybylkowski A, Czlonkowska A, Czlonkowski A (2009) Age- and sex-differences in the nitric oxide synthase expression and dopamine concentration in the murine model of Parkinson's disease induced by 1-methyl-4-phenyl-1,2,3,6-tetrahydropyridine. Brain Res 1261:7–19.

Kahle PJ, Neumann M, Ozmen L, Haass C (2000a) Physiology and pathophysiology of alpha-synuclein: cell culture and transgenic animal models based on a Parkinson's disease-associated protein. Ann NY Acad Sci 920:33–41.

Kahle PJ, Neumann M, Ozmen L, Muller V, Jacobsen H, Schindzielorz A, Okochi M, Leimer U, van Der Putten H, Probst A, Kremmer E, Kretzschmar HA, Haass C (2000b) Subcellular localization of wild-type and Parkinson's disease-associated mutant alpha-synuclein in human and transgenic mouse brain. J Neurosci 20:6365–6373.

Kam TI, et al. (2018) Poly(ADP-ribose) drives pathologic alpha-synuclein neurodegeneration in Parkinson's disease. Science 362:eaat8407.

Kim S, Kwon SH, Kam TI, Panicker N, Karuppagounder SS, Lee S, Lee JH, Kim WR, Kook M, Foss CA, Shen C, Lee H, Kulkarni S, Pasricha PJ, Lee G, Pomper MG, Dawson VL, Dawson TM, Ko HS (2019) Transneuronal propagation of pathologic alpha-synuclein from the gut to the brain models Parkinson's disease. Neuron 103:627–641.e7.

Kornau HC, Schenker LT, Kennedy MB, Seeburg PH (1995) Domain interaction between NMDA receptor subunits and the postsynaptic density protein PSD-95. Science 269:1737–1740.

Kramer ML, Schulz-Schaeffer WJ (2007) Presynaptic alpha-synuclein aggregates, not Lewy bodies, cause neurodegeneration in dementia with Lewy bodies. J Neurosci 27:1405–1410.

Krishnan S, Chi EY, Wood SJ, Kendrick BS, Li C, Garzon-Rodriguez W, Wypych J, Randolph TW, Narhi LO, Biere AL, Citron M, Carpenter JF (2003) Oxidative dimer formation is the critical rate-limiting step for Parkinson's disease α-synuclein fibrillogenesis. Biochemistry 42:829–837.

Lipton SA, Choi YB, Pan ZH, Lei SZ, Chen HS, Sucher NJ, Loscalzo J, Singel DJ, Stamler JS (1993) A redox-based mechanism for the neuroprotective and neurodestructive effects of nitric oxide and related nitroso-compounds. Nature 364:626–632.

Liu Y, Lee JW, Ackerman SL (2015) Mutations in the microtubule-associated protein 1A (Map1a) gene cause Purkinje cell degeneration. J Neurosci 35:4587–4598.

Luk KC, Kehm V, Carroll J, Zhang B, O'Brien P, Trojanowski JQ, Lee VM (2012) Pathological alpha-synuclein transmission initiates Parkinson-like neurodegeneration in nontransgenic mice. Science 338:949–953.

Luk KC, Song C, O'Brien P, Stieber A, Branch JR, Brunden KR, Trojanowski JQ, Lee VM (2009) Exogenous alpha-synuclein fibrils seed the formation of Lewy body-like intracellular inclusions in cultured cells. Proc Natl Acad Sci USA 106:20051–20056.

Mahul-Mellier AL, Burtscher J, Maharjan N, Weerens L, Croisier M, Kuttler F, Leleu M, Knott GW, Lashuel HA (2020) The process of Lewy body formation, rather than simply alpha-synuclein fibrillization, is one of the major drivers of neurodegeneration. Proc Natl Acad Sci USA 117:4971–4982.

Mnatsakanyan R, Markoutsa S, Walbrunn K, Roos A, Verhelst SH, Zahedi RP (2019) Proteome-wide detection of S-nitrosylation targets and motifs using bioorthogonal cleavable-linker-based enrichment and switch technique. Nat Commun 10:2195.

Monti DA, Zabrecky G, Kremens D, Liang TW, Wintering NA, Bazzan AJ, Zhong L, Bowens BK, Chervoneva I, Intenzo C, Newberg AB

(2019) N-Acetyl cysteine is associated with dopaminergic improvement in Parkinson's disease. Clin Pharmacol Ther 106:884–890.

Musgrove RE, Helwig M, Bae EJ, Aboutalebi H, Lee SJ, Ulusoy A, Di Monte DA (2019) Oxidative stress in vagal neurons promotes parkinsonian pathology and intercellular alpha-synuclein transfer. J Clin Invest 129:3738–3753.

Nakamura T, Tu S, Akhtar MW, Sunico CR, Okamoto S, Lipton SA (2013) Aberrant protein s-nitrosylation in neurodegenerative diseases. Neuron 78:596–614.

Norris EH, Giasson BI, Ischiropoulos H, Lee VM (2003) Effects of oxidative and nitrative challenges on alpha-synuclein fibrillogenesis involve distinct mechanisms of protein modifications. J Biol Chem 278:27230–27240.

Nuber S, Rajsombath M, Minakaki G, Winkler J, Muller CP, Ericsson M, Caldarone B, Dettmer U, Selkoe DJ (2018) Abrogating native alpha-synuclein tetramers in mice causes a L-DOPA-responsive motor syndrome closely resembling Parkinson's disease. Neuron 100:75–90.e5.

Paxinou E, Chen Q, Weisse M, Giasson BI, Norris EH, Rueter SM, Trojanowski JQ, Lee VM, Ischiropoulos H (2001) Induction of α-synuclein aggregation by intracellular nitrative insult. J Neurosci 21:8053–8061.

Picon-Pages P, Garcia-Buendia J, Muñoz FJ (2019) Functions and dysfunctions of nitric oxide in brain. Biochim Biophys Acta Mol Basis Dis 1865:1949–1967.

Reese ML, Dakoji S, Bredt DS, Dotsch V (2007) The guanylate kinase domain of the MAGUK PSD-95 binds dynamically to a conserved motif in MAP1a. Nat Struct Mol Biol 14:155–163.

Rushworth GF, Megson IL (2014) Existing and potential therapeutic uses for N-acetylcysteine: the need for conversion to intracellular glutathione for antioxidant benefits. Pharmacol Ther 141:150–159.

Ryan SD, et al. (2013) Isogenic human iPSC Parkinson's model shows nitrosative stress-induced dysfunction in MEF2-PGC1alpha transcription. Cell 155:1351–1364.

Seneviratne U, Nott A, Bhat VB, Ravindra KC, Wishnok JS, Tsai LH, Tannenbaum SR (2016) S-nitrosation of proteins relevant to Alzheimer's disease during early stages of neurodegeneration. Proc Natl Acad Sci USA 113:4152–4157.

Sevcsik E, Trexler AJ, Dunn JM, Rhoades E (2011) Allostery in a disordered protein: oxidative modifications to alpha-synuclein act distally to regulate membrane binding. J Am Chem Soc 133:7152–7158.

Shrivastava AN, Bousset L, Renner M, Redeker V, Savistchenko J, Triller A, Melki R (2020) Differential membrane binding and seeding of distinct alpha-synuclein fibrillar polymorphs. Biophys J 118:1301–1320.

Stamler JS, Simon DI, Osborne JA, Mullins ME, Jaraki O, Michel T, Singel DJ, Loscalzo J (1992) S-nitrosylation of proteins with nitric oxide: synthesis and characterization of biologically active compounds. Proc Natl Acad Sci USA 89:444–448.

Stykel MG, Kirby MP, Czaniecki C, Humphries K, Ryan TL, Ryan SD (2018) Nitration of microtubules blocks axonal mitochondrial transport in a human pluripotent stem cell model of Parkinson's disease. FASEB J 32:5350–5364.

Sulzer D, Edwards RH (2019) The physiological role of alpha-synuclein and its relationship to Parkinson's disease. J Neurochem 150:475–486.

Takei Y, Kikkawa YS, Atapour N, Hensch TK, Hirokawa N (2015) Defects in synaptic plasticity, reduced NMDA-receptor transport, and instability of postsynaptic density proteins in mice lacking microtubule-associated protein 1A. J Neurosci 35:15539–15554.

Tapias V, Hu X, Luk KC, Sanders LH, Lee VM, Greenamyre JT (2017) Synthetic alpha-synuclein fibrils cause mitochondrial impairment and selective dopamine neurodegeneration in part via iNOS-mediated nitric oxide production. Cell Mol Life Sci 74:2851–2874.

Trudler D, Sanz-Blasco S, Eisele YS, Ghatak S, Bodhinathan K, Akhtar MW, Lynch WP, Pina-Crespo JC, Talantova M, Kelly JW, Lipton SA (2021) alpha-Synuclein oligomers induce glutamate release from astrocytes and excessive extrasynaptic NMDAR activity in neurons, thus contributing to synapse loss. J Neurosci 41:2264–2273.

Uversky VN, Yamin G, Munishkina LA, Karymov MA, Millett IS, Doniach S, Lyubchenko YL, Fink AL (2005) Effects of nitration on the structure and aggregation of alpha-synuclein. Brain Res Mol Brain Res 134:84–102.

Volpicelli-Daley LA, Luk KC, Patel TP, Tanik SA, Riddle DM, Stieber A, Meaney DF, Trojanowski JQ, Lee VM (2011) Exogenous alpha-synuclein fibrils induce Lewy body pathology leading to synaptic dysfunction and neuron death. Neuron 72:57–71.

Volpicelli-Daley LA, Luk KC, Lee VM (2014) Addition of exogenous alpha-synuclein preformed fibrils to primary neuronal cultures to seed recruitment of endogenous alpha-synuclein to Lewy body and Lewy neurite-like aggregates. Nat Protoc 9:2135–2146.

Warde-Farley D, Donaldson SL, Comes O, Zuberi K, Badrawi R, Chao P, Franz M, Grouios C, Kazi F, Lopes CT, Maitland A, Mostafavi S, Montojo J, Shao Q, Wright G, Bader GD, Morris Q (2010) The GeneMANIA prediction server: biological network integration for gene prioritization and predicting gene function. Nucleic Acids Res 38:W214–W220.

Watanabe Y, Kato H, Araki T (2008) Protective action of neuronal nitric oxide synthase inhibitor in the MPTP mouse model of Parkinson's disease. Metab Brain Dis 23:51–69.

Withers GS, George JM, Banker GA, Clayton DF (1997) Delayed localization of synelfin (synuclein, NACP) to presynaptic terminals in cultured rat hippocampal neurons. Brain Res Dev Brain Res 99:87–94.

Wong YC, Krainc D (2017) α-Synuclein toxicity in neurodegeneration: mechanism and therapeutic strategies. Nat Med 23:1–13.

Wu Q, Takano H, Riddle DM, Trojanowski JQ, Coulter DA, Lee VM (2019) α-Synuclein (alphaSyn) preformed fibrils induce endogenous alphaSyn aggregation, compromise synaptic activity and enhance synapse loss in cultured excitatory hippocampal neurons. J Neurosci 39:5080–5094.

Yang J, Hertz E, Zhang X, Leinartaite L, Lundius EG, Li J, Svenningsson P (2016) Overexpression of alpha-synuclein simultaneously increases glutamate NMDA receptor phosphorylation and reduces glucocerebrosidase activity. Neurosci Lett 611:51–58.

Zahid S, Khan R, Oellerich M, Ahmed N, Asif AR (2014) Differential S-nitrosylation of proteins in Alzheimer's disease. Neuroscience 256:126–136.

Zaręba-Kozioł M, Szwajda A, Dadlez M, Wysłouch-Cieszyńska A, Lalowski M (2014) Global analysis of S-nitrosylation sites in the wild type (APP) transgenic mouse brain: clues for synaptic pathology. Mol Cell Proteomics 13:2288–2305.

Zhang L, Zhang C, Zhu Y, Cai Q, Chan P, Ueda K, Yu S, Yang H (2008) Semi-quantitative analysis of alpha-synuclein in subcellular pools of rat brain neurons: an immunogold electron microscopic study using a C-terminal specific monoclonal antibody. Brain Res 1244:40–52.

Zhu J, Gao W, Shan X, Wang C, Wang H, Shao Z, Dou S, Jiang Y, Wang C, Cheng B (2020) Apelin-36 mediates neuroprotective effects by regulating oxidative stress, autophagy and apoptosis in MPTP-induced Parkinson's disease model mice. Brain Res 1726:146493.